


Tectonic and lithological controls on denudation rates in the central Bolivian Andes

Journal Article**Author(s):**

Kober, Florian; Zeilinger, Gerold; Hippe, Kristina; Marc, Oliver; Lenzioch, T.; Grischott, Reto; [Christl, Marcus](#) ; Kubik, Peter W.; Zolá, Ramiro S.P.

Publication date:

2015-08-30

Permanent link:

<https://doi.org/10.3929/ethz-b-000104786>

Rights / license:

[Creative Commons Attribution-NonCommercial-NoDerivatives 4.0 International](#)

Originally published in:

Tectonophysics 657, <https://doi.org/10.1016/j.tecto.2015.06.037>



Tectonic and lithological controls on denudation rates in the central Bolivian Andes



F. Kober^{a,b,*}, G. Zeilinger^c, K. Hippe^{d,e}, O. Marc^{b,c}, T. Lenzioch^c, R. Grischott^a, M. Christl^d, P.W. Kubik^d, R. Zola^f

^a Geological Institute, ETH Zürich, Sonneggstrasse 5, 8092 Zürich, Switzerland

^b Helmholtz-Zentrum Potsdam - Deutsches GeoForschungsZentrum, Telegrafenberg, D-14473 Potsdam, Germany

^c Universität Potsdam, Institut für Erd- und Umweltwissenschaften, Karl-Liebknecht-Strasse 24, 14476 Potsdam, Germany

^d Laboratory of Ion Beam Physics, ETH Zürich, 8093 Zürich, Switzerland

^e Institute of Geochemistry and Petrology, ETH Zürich, Clausiusstrasse 25, 8092 Zürich, Switzerland

^f Instituto de Hidráulica e Hidrología, Universidad Mayor de San Andrés, La Paz, Bolivia

ARTICLE INFO

Article history:

Received 26 November 2014

Received in revised form 16 June 2015

Accepted 25 June 2015

Available online 29 July 2015

Keywords:

Rio Grande
seismicity
uplift
rock strength
cosmogenic nuclides
denudation

ABSTRACT

The topographic signature of a mountain belt depends on the interplay of tectonic, climatic and erosional processes, whose relative importance changes over times, while quantifying these processes and their rates at specific times remains a challenge. The eastern Andes of central Bolivia offer a natural laboratory in which such interplay has been debated. Here, we investigate the Rio Grande catchment which crosses orthogonally the eastern Andes orogen from the Eastern Cordillera into the Subandean Zone, exhibiting a catchment relief of up to 5000 m. Despite an enhanced tectonic activity in the Subandes, local relief, mean and modal slopes and channel steepness indices are largely similar compared to the Eastern Cordillera and the intervening Interandean Zone. Nevertheless, a dataset of 57 new cosmogenic ¹⁰Be and ²⁶Al catchment wide denudation rates from the Rio Grande catchment reveals up to one order of magnitude higher denudation rates in the Subandean Zone (mean 0.8 mm/yr) compared to the upstream physiographic regions. We infer that tectonic activity in the thrusting dominated Subandean belt causes higher denudation rates based on cumulative rock uplift investigations and due to the absence of a pronounced climate gradient. Furthermore, the lower rock strength of the Subandean sedimentary units correlates with mean slopes similar to the ones of the Eastern Cordillera and Interandean Zone, highlighting the fact, that lithology and rock strength can control high denudation rates at low slopes.

Low denudation rates measured at the outlet of the Rio Grande catchment (Abapo) are interpreted to be a result of a biased cosmogenic nuclide mixing that is dominated by headwater signals from the Eastern Cordillera and the Interandean zone and limited catchment sediment connectivity in the lower river reaches. Therefore, comparisons of short- (i.e., sediment yield) and millennial denudation rates require caution when postulating tectonic and/or climatic forcing without detailed studies.

© 2015 The Authors. Published by Elsevier B.V. This is an open access article under the CC BY-NC-ND license (<http://creativecommons.org/licenses/by-nc-nd/4.0/>).

1. Introduction

Mountain ranges stand out because of their relief. In general, relief is formed due to (plate) tectonic forcing shifting a landscape into a constructional topographic state. When critical elevations and slope values are approached, erosion begins to significantly contribute to landscape development. Topography then modulates air circulation and precipitation patterns (orographic rainfall) which in turn may enhance the effects on erosion (Roe et al., 2002). Eventually, tectonic

influx and erosional outflux are balanced, shifting a mountain range into a topographic steady state (Montgomery, 2001). With ceasing tectonic forcing, persistent erosional processes outpace tectonic processes and set the mountain range into a destructional topographic state with decreasing relief. Studying such relief – erosion relationships and finding causal links between tectonics, climate and erosion can be performed by analysing topographic metrics (Champagnac et al., 2012) and quantifying exhumation and denudation rates (Burbank, 2002). However, it has been challenging to quantify the conditions and magnitudes of a tectonic, erosional, topographic transient or steady state and the timescales associated with them – a crucial prerequisite in the understanding and modelling of landscape evolution. Numerous parameters have to be considered because the construction of topography is

* Corresponding author at: Nagra, Hardstrasse 73, 5430 Wettingen, Switzerland. Tel.: +41 564371336; fax: +41 44 6321422.

E-mail addresses: kober@erdw.ethz.ch, florian.kober@nagra.ch (F. Kober).

spatially and temporarily variable and multiple evolutionary states may simultaneously exist or have variable response times. Furthermore, measuring uplift or erosion rates depends on various methods that are sensitive to spatial and temporal scales or have variable responses to transient processes (Schumm and Lichty, 1965). Moreover, common tectonic (e.g., seismicity, strain rates) and climatic (e.g., temperature, rainfall) parameters potentially preserved in a landscape are gathered over modern or historical timescales and may not be representative over longer timescales.

In order to illustrate the debate, common characteristics of tectonically active landscape studies are a steep relief, threshold slopes and mass-wasting processes (Korup et al., 2010; Montgomery and Brandon, 2002; Schmidt and Montgomery, 1995). Threshold slopes are referred to as being on the order of 25° or higher (DiBiase et al., 2010; Ouimet et al., 2009) with erosion rates increasing nonlinearly above this threshold value. However, it has also been shown that younger sedimentary sequences, lower grade exhumed structural depth levels or dip-slip/anti-dip-slip conditions can also yield threshold slopes with values <25° but under high denudation rates (Dadson et al., 2003; Duvall et al., 2004; Korup and Weidinger, 2011; Schmidt and Montgomery, 1995).

For the central Andes, it has been suggested that, on a regional scale, the geodynamic evolution and climate play a significant role in landscape evolution (Hilley and Coutand, 2009; Montgomery et al., 2001; Strecker et al., 2007). Studies on various spatial and temporal scales of uplift or denudation rates in the central Andes, however, identified different driving forces, amongst them regional tectonics and rock properties (Aalto et al., 2006; Insel et al., 2010; Safran et al., 2005; Whipple and Gasparini, 2014). In general, relief, slopes, orographic precipitation and denudation rates have higher values in the north of the Bolivian orocline (18°S), while south of it, these parameters reflect lower values (Masek et al., 1994; Montgomery et al., 2001). Here, we study the eastern Andes south of 18°S in detail by highlighting the complex interactions in mountain belt evolution with a compilation of various topographic metrics for the Rio Grande catchment in combination with a cosmogenic nuclide (¹⁰Be and ²⁶Al) derived denudation rate dataset. The data are supplemented by previously acquired decadal denudation rates from sediment yield data (Guyot et al., 1994), and geo-thermochronologic estimates on million year timescales (Barnes et al., 2008). We assess the tectonic imprint, its reflection in cumulative seismic uplift and its potential effects on denudation rates in the Subandean Zone of the central Bolivian Andes, where a migrating tectonic front and the current shallow seismic activity constantly rejuvenates the landscape (Barnes et al., 2012; Horton, 1999; Montgomery et al., 2001). Consequently, denudation rates should be highest there. We will show that for the entire dataset common topographic metrics typical for a tectonic forcing reveal no distinct correlations with denudation rates in the eastern central Andes, as observed elsewhere in active tectonic regions. This is despite the fact that the denudation rates vary by an order of magnitude, similar to tectonic activity. Moreover, we will discuss the possible occurrence of threshold hillslope angles in the Subandes relating to the limited rock strength of young sedimentary sequences.

2. Geology & Tectonics

The Rio Grande catchment upstream of Abapo (Fig. 1) covers an area of 58939 km² over an altitude ranging from 400 to 5150 m asl. From west to east, five physiographic provinces can be distinguished (Fig. 1): the low relief Altiplano plateau, the Eastern Cordillera (EC), the Interandean Zone (IAZ) and the Subandean zone (SA), grading into the low-relief – flat Chaco plain (Amazon basin) (Soruco, 2000). The formation of these large-scale physiographic regions has been controlled by duplexing and stacking of two thrust sheets (McQuarrie, 2002). The development of the fold and thrust belt occurred by Cenozoic crustal shortening and thickening forced by the subduction of the Nazca plate below the South American plate (Isacks, 1988). The EC, composed of marine metasedimentary siliciclastic rocks of Palaeozoic age,

experienced a period of intense shortening and exhumation between the Late Oligocene and Miocene (Echavarría et al., 2003; Horton and DeCelles, 1997). The IAZ and SA form an east-vergent thin-skinned fold and thrust belt in a retroarc position and comprise Palaeozoic and Mesozoic units (McQuarrie, 2002). Farther east, the structures of the Subandean zone progressively include Neogene continental strata of the low relief Chaco foreland basin. The deformation stepped from the SA into the Chaco foreland basin at c. 8 Myr by forming wider and gentler anticlines on top of a critical taper (Barnes et al., 2012; Echavarría et al., 2003; Uba et al., 2006). Present-day deformation and earthquake activity is located in a few frontal thrusts (Oncken et al., 2012) with aseismic shortening within the remaining parts of the SA (Brooks et al., 2011). Current GPS-shortening rates are 6.5 – 13 mm/yr (Barnes et al., 2008, 2012; Brooks et al., 2011; McQuarrie, 2002; Oncken et al., 2012).

Uplift rates based on geodetic, paleomagnetic and structural data are on the order of 10–100 mm/ky for the EC and IAZ and 500 – 2000 mm/ky for the SA (Lamb, 2000), implying a 10-fold increase between the EC/IAZ and SA. The SA are characterized by recent seismicity associated with dip-slip (thrust) events whereas the Cochabamba province (EC) is dominated by slightly oblique strike-slip events (Brooks et al., 2011; Echavarría et al., 2003; Rhea et al., 2010; Vega and Buforn, 1991), acknowledging the regional influence of the bending of the eastern Andes at ~18°S (Isacks, 1988).

South of 18°S, long-term denudation rates based on apatite fission track data yield rates of ~ 200 ± 70 mm/ky for the EC, ~150 ± 60 mm/ky for the IAZ and ~ 310 ± 110 mm/ky for the SA (Insel et al., 2010). For the EC and the IAZ they broadly match with the estimates on uplift, while they are significantly lower for the SA. Denudation rates increase from 10⁶ to 10³ yr timescales with no concomitant systematic correlations with morphometric parameters or precipitation changes (Insel et al., 2010). The temporal variability in these denudation rates was attributed to Holocene climate changes, while an observed spatial variability was proposed to reflect local tectonic variations (Insel et al., 2010). Sediment gauging data revealed high sediment load rates in the Rio Grande upstream of Abapo with seasonal and inter-annual variability on sediment transport processes (Guyot et al., 1994; Guyot et al., 1996). According to Aalto et al. (2006), lithology and rock erodibility control some variance on decadal denudation rates, but do not control millennial denudation rates (Insel et al., 2010; Safran et al., 2005). Bookhagen and Strecker (2012) point out the importance of climatic parameters on the efficiency of surface processes through time. By coupling the specific stream power concept with their cosmogenic denudation rates their data are best explained. Today, hillslopes in the EC and IAZ are thinly soil covered, mainly characterized by regolith, whereas in the SA soils up to 1 m thick are common (Coppus, 2002).

3. Climate

The Eastern Andes act as a barrier for moisture from the Amazon basin and impose an orographic rainfall pattern. However, south of the Bolivian Bend, at ~ 18°S where the fold and thrust belt widens, the precipitation pattern is characterized only by a gentle modern E-W gradient (Bookhagen and Strecker, 2008; Díaz et al., 2010; Masek et al., 1994). Since the main moisture transport across the southern Amazon basin is WSW oriented, the Bolivian Bend shields the area just S of it from strong precipitation. Mean annual precipitation ranges from 200–1200 mm/yr (Fig. 1, Bookhagen and Strecker, 2008). With altitude, the amount of rainfall decreases gently and vegetation cover declines rapidly.

4. Methods

4.1. Sampling strategy, cosmogenic nuclide analysis, denudation and sediment flux estimations

Sediment sampling for establishing cosmogenic nuclide concentrations took place in sub-catchments of each physiographic region along

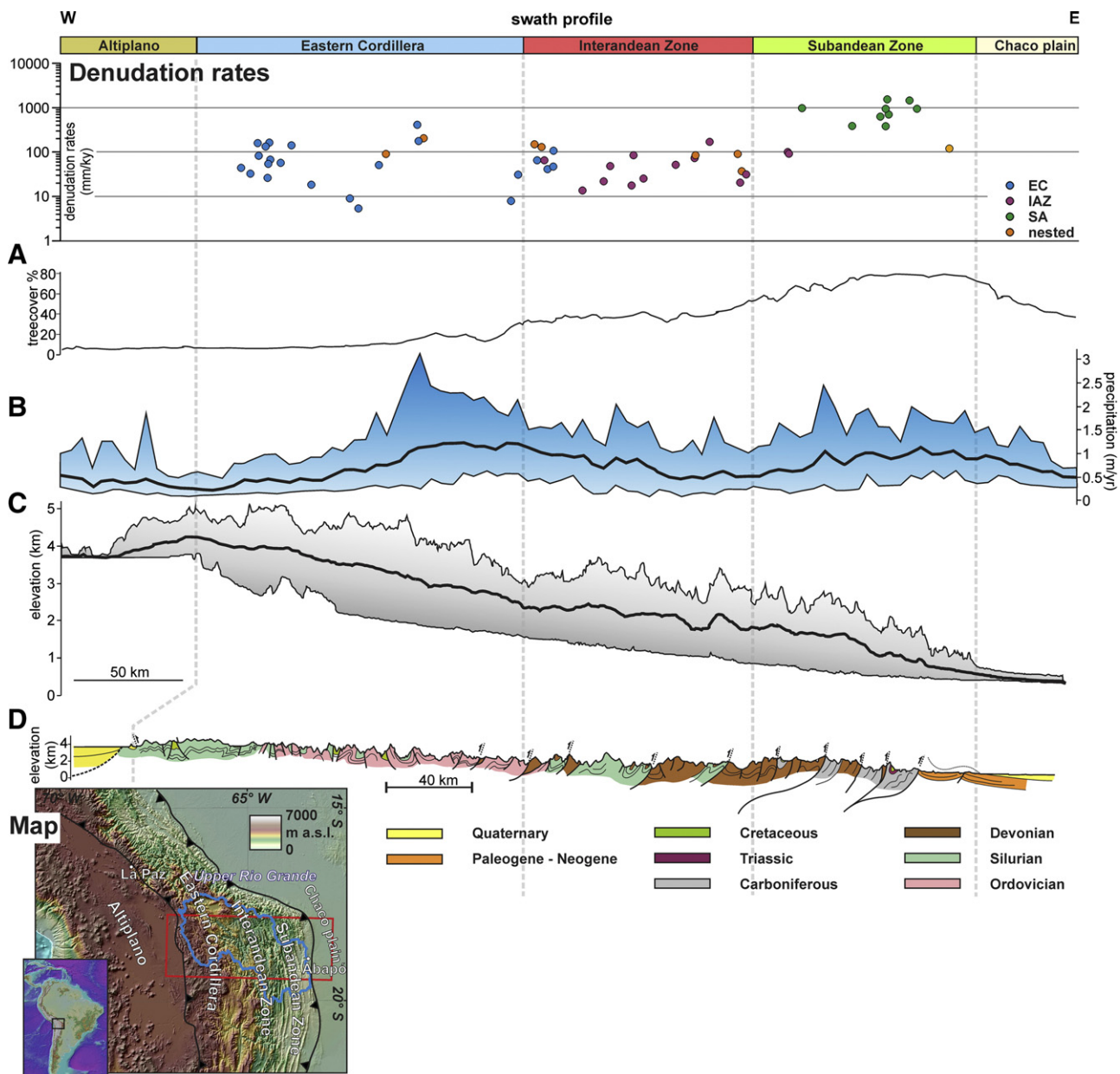


Fig. 1. Location of the upper Rio Grande catchment on the eastern flank of the central Andes of Bolivia (map, GTOPO30 and SRTM DEM). The upper Rio Grande is shown with the physiographic regions of the Eastern Cordillera, the Interandean Zone and the Subandes. Cosmogenic nuclide derived denudation rates are shown in the context of vegetation (A) (Source: DeFries et al., 2000), precipitation swath (B) (Source: TRMM data, Bookhagen and Strecker, 2008, red box in map shows swath extent), topographic swath (C) (Source: ASTER G-DEM data V2, ASTER GDEM is a product of METI and NASA), and in the geological context (D) (Guarachi et al., 2001).

the Rio Grande (Figs. 1 and 2), where we systematically defined the sampled catchment size by a 6th Strahler order (mean size $\sim 700 \text{ km}^2$). Additionally, we collected trunk-stream sediment samples that integrate sediment from several sub-catchments. These trunk-stream samples are classified as “nested samples” (Fig. 2) and are taken in the vicinity of locations sampled by Guyot et al. (1994) for sediment yield estimations. The individual catchments comprise various stratigraphic units that are composed of similar lithologies, mostly conglomerates, sandstones, silts, shales and some volcanic rocks.

Samples were taken from the modern riverbed and sieved for a grain size of 0.25–1 mm. Samples that did not contain sufficient amounts of this grain-size fraction were analysed for the fraction $< 0.25 \text{ mm}$ (Table 1, Appendix) assuming that no significant grain size dependence of the cosmogenic nuclide concentration exists at this grain size scale (Insel et al., 2010; Safran et al., 2005). Physical and chemical cleaning

and dissolution procedures are outlined in Hippe et al. (2012). The $^{10}\text{Be}/^9\text{Be}$ ratios were measured on the compact ETH AMS TANDY system (Müller et al., 2010) relative to the standard S2007N with a nominal $^{10}\text{Be}/^9\text{Be}$ value of 28.1×10^{-12} (Christl et al., 2013). A mean blank ratio of $(3.3 \pm 0.4) \times 10^{-15}$ ($n = 3$), which mostly represents the $^{10}\text{Be}/^9\text{Be}$ ratio of the carrier material, was subtracted from sample measurements. Prior to Be-separation, an aliquot was taken from the sample solution for the measurement of the Al concentration. $^{26}\text{Al}/^{27}\text{Al}$ ratios were measured at the ETH AMS TANDEM facility (Christl et al., 2013). The Al concentration was determined by standard addition to the untreated aliquots of the dissolved samples using inductively coupled plasma mass spectrometry (ICP-MS). Denudation rates were calculated with the CRONUS-Earth online calculator version 2.2. using the Stone (2000) scaling scheme (Balco et al., 2008), and assuming a ^{10}Be half-life of $1.387 \pm 0.012 \text{ Ma}$ (Chmeleff et al., 2010; Korschinek et al., 2010) with topographic shielding corrections (Codilean, 2006). For

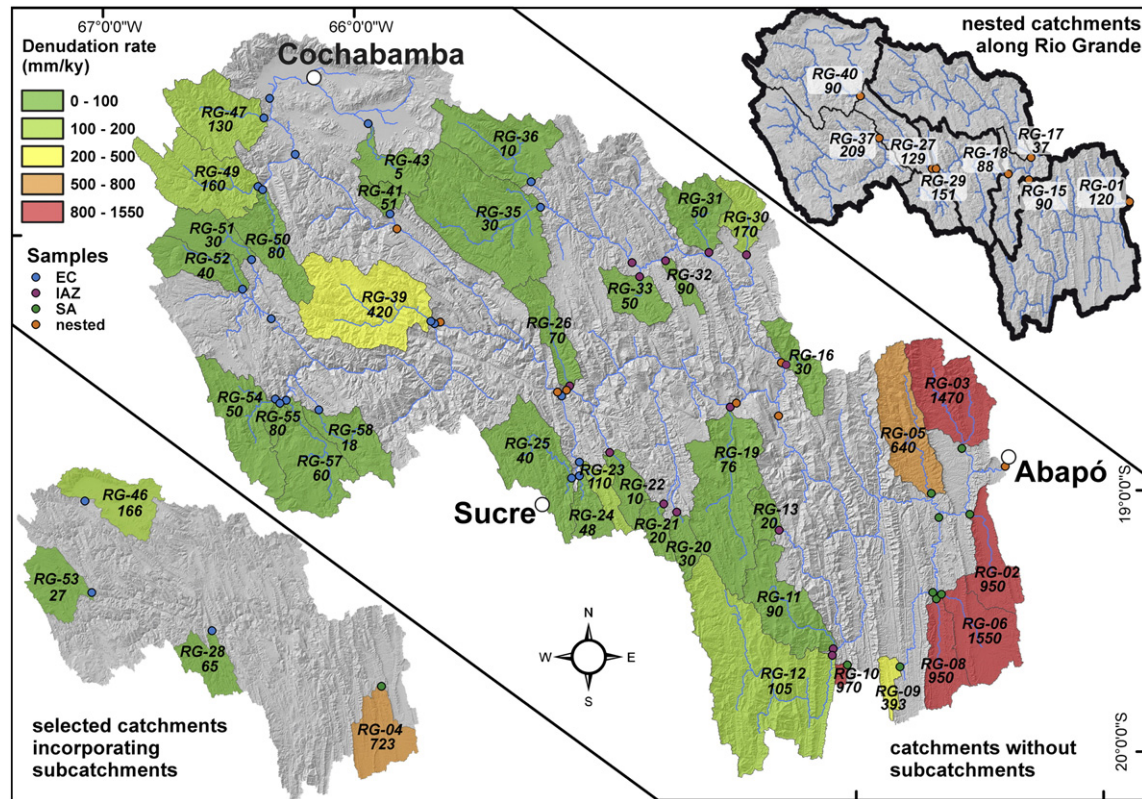


Fig. 2. Spatial distribution of cosmogenic nuclide derived denudation rates in the upper Rio Grande catchment with respect to their physiographic distribution. Level 1 catchment sizes are comparable to a Strahler stream order 6 (average area – 700 km²); level 3 catchments (lower left) integrate over two or more level 1 catchments. The nested samples, shown in the upper right map, follow the main trunk stream and form a series of lower level catchments. Thickness of the line outlining the catchments is increasing with increasing Strahler order.

comparison, previously published denudation rates from Safran et al. (2005), Wittmann et al. (2009) and Insel et al. (2010) for catchments > 100 km² were recalculated following the scheme outlined above. Those recalculated denudation rates are up to 20% lower than previous calculations, which is mainly due to a lower ¹⁰Be production rate following revision of the ¹⁰Be decay constant. To compare with cosmogenic nuclide data, sediment gauging data (Aalto et al., 2006; Guyot et al., 1994) have been converted into denudation rates.

4.2. Geomorphic analysis

In order to identify landscape controls on denudation rates, various standard geomorphic metrics were analysed using ASTER Global Elevation Maps (GDEM, 30 m resolution, ASTER G-DEM data V2) and SRTM V4 data (90 m resolution; Jarvis et al., 2008). Both datasets have horizontal and vertical errors in the range of tens of meters. The difference between both datasets for the basic morphological parameters (mean elevation, mean slope, and mean (local) relief) falls within the accuracy of the datasets. In order to enhance resolution, the GDEM dataset was used for calculations of the hypsometric integral (HI), drainage density (Dd) and the normalized channel steepness (k_{sn}). The quality of the GDEM dataset within the Rio Grande catchment justifies the calculation of the geomorphic parameters based on this 30 m resolution dataset. The comparison with the SRTM dataset (90 m resolution) reveals that the investigated geomorphic parameters are not scale dependent within the given range of resolution. In order to yield spatially higher resolved results we prefer the calculation of the parameters HI, k_{sn} and Dd with the GDEM dataset.

The characteristics of the applied methods are briefly outlined in the following:

Information on *catchment scale relief* was studied by a scale dependent analysis of the local relief using search window diameters of 3, 5, 6 and 10 km. The *local relief* estimates correspond to processes in

small scale catchments, which integrate processes on hillslopes and in tributaries, while mountain relief reflects range-scale processes. For a quantitative comparison of landscape processes, we computed the *slope distribution*, assuming that the skewness of this distribution reveals the predominance of continuous (hillslope) versus episodic (mass wasting) landscape processes (DiBiase et al., 2012; Wolinsky and Pratson, 2005). The basin *hypsometry index* (HI) relates the horizontal cross-sectional area of a drainage basin to its relative elevation above the basin mouth. It represents the degree of landscape dissection and the geomorphic maturity of evolving landscapes (Ohmori, 1993; Strahler, 1952). It combines form and processes, thus its value is rather of qualitative than quantitative relevance. *Drainage density* (D_d) is defined by the total length of stream channels per unit area of the basin (Moglen et al., 1998) and describes the texture of a stream network in a drainage basin. We calculated the catchment scale D_{dc} (*drainage density catchment scale*) by summing up all channels in the catchment using a stream raster with an upper threshold of 1 km² and compared it to a local D_{dl} (*local drainage density*) using the same river network analysed by a river length/circle relation (diameter 5 km). *Channel steepness* characterizes the coupling of topography and rock uplift, climate and erodibility (Wobus et al., 2006), where the upstream area and its local slope are compared to a graded stream profile. We chose a reference concavity of 0.45 to derive a normalized *channel steepness* (k_{sn}) index with a critical drainage area of > 1 km². *Channel sinuosity* is a marker for channel slope variations (the ratio of valley slope to channel gradient), and is sensitive to aggradation and incision cycles (Schumm and Lichty, 1965). It reflects the ability of a channel to adjust to tectonic activity. We calculated channel sinuosity for river segments between confluences defined by Strahler orders, considering only river segments longer than 500 m in order to avoid artefacts caused by extraction of rivers from DEMs.

We analysed the shape of *longitudinal river-channel profiles* which, in tectonically active settings, typically have concave-upward shapes

revealing a comparably higher tectonic activity, unless confluences or erodibility contrasts perturb this pattern (Burbank & Anderson, 2001). They typically have concomitant excursions in *channels steepness* indices. Additionally, we compared the *preferred orientation* of fluvial drainages and their relation to tectonically pre-defined structural orientations. Structures were extracted from the geological map (Guarachi et al., 2001) and assigned a strike direction. Similarly, all channels extracted from the GDEM-DEM have been assigned with their flow direction. All data have been plotted in Rose diagrams using bins of 10°.

In order to account for the effects of lithology, rock strength and erodibility, a proxy for erodibility was computed by assigning a *Probst lithologic index* (PLI, see Ludwig and Probst, 1998) to lithologies, following Aalto et al. (2006). This resulted in a classification into strong Palaeozoic sedimentary rocks (PLI 2 to 4), weak Mesozoic rocks (PLI 5 to 6), very weak Cenozoic rocks (PLI 9 to 11), and unconsolidated Quaternary sediments (PLI 13). The PLI was obtained at the catchment scale in taking the mean PLI of the different lithologies weighted by their relative area on the geological map. Hereby, a high PLI value indicates both, high sensitivity to weathering and low compressive strength (Aalto et al., 2006).

Mean annual precipitation was calculated using TRMM-data (Huffman et al., 2007) with a temporal cover of 10 years, a 5 x 5 km spatial grid resolution, and a validation with rainfall-gauged ground stations (Bookhagen and Strecker, 2008). The impact of vegetation and anthropogenic perturbation on denudation rates was verified by compiling data on land use (De Fries et al., 1998) and a *tree cover index* (Defries et al., 2000). Hereby, we acknowledge that the degree of tree canopy may not fully reflect weathering and erosional processes (Vanacker et al., 2007).

4.3. Cumulative seismic moment and volume uplift

In order to test the spatial variability of denudation rates as a function of tectonic activity, an analysis of the cumulative seismic moment and uplifted volume was performed. Between 17.2° - 20°S and 62° - 66°W, crustal earthquakes with magnitudes higher than 5 and depths shallower than ~40 km were considered. Surface effects from deeper earthquakes are unlikely and thus neglected (e.g., Weston et al., 2011). Eleven instrumentally recorded earthquakes (between 1969 and 2011) with constrained focal mechanism and seismic moments were compiled (Dziewonski et al., 1981; Ekström et al., 2012; Vega and Buforn, 1991). Using dislocation theory, Okada (1985) has developed analytical formulas expressing surface deformation based on the slip applied on a fault plane of a given length, width, dip, rake and depth. This expression has proven very efficient to invert surface deformation measured by InSAR into slip on the fault plane (Weston et al., 2011). By integrating the vertical component of the deformation field we obtain a net seismically uplifted volume over an area scaling with 1 to 2 of the fault lengths (i.e., 10 by 10 km to 20 by 20 km for a typical Mw 6, for shallow or deeper earthquakes, respectively). Fault dimensions and average slip were determined from the moment using scaling relationships (Leonard, 2010), while depth and average dip and rake were based on focal mechanisms. The uplifted volume was constructed by integrating all vertical surface displacement of amplitude greater than 0.5% of the maximum, thus, accounting for near field subsidence but excluding far-field elastic oscillations and avoiding a solution dependence on the numerical domain size.

As shown by Vega and Buforn (1991), earthquakes in the greater Rio Grande region can be split into steep, oblique strike-slip events near Cochabamba, and thrust events at the boundary between the Subandean zone and the Chaco Plain. This reflects the close geographic position of the studied region to the Bolivian orocline bend at 18°S. By considering the spatial pattern of seismicity, both historic and modern (Fig. 7), two longitudinal stripes are evident, with a relatively quiet

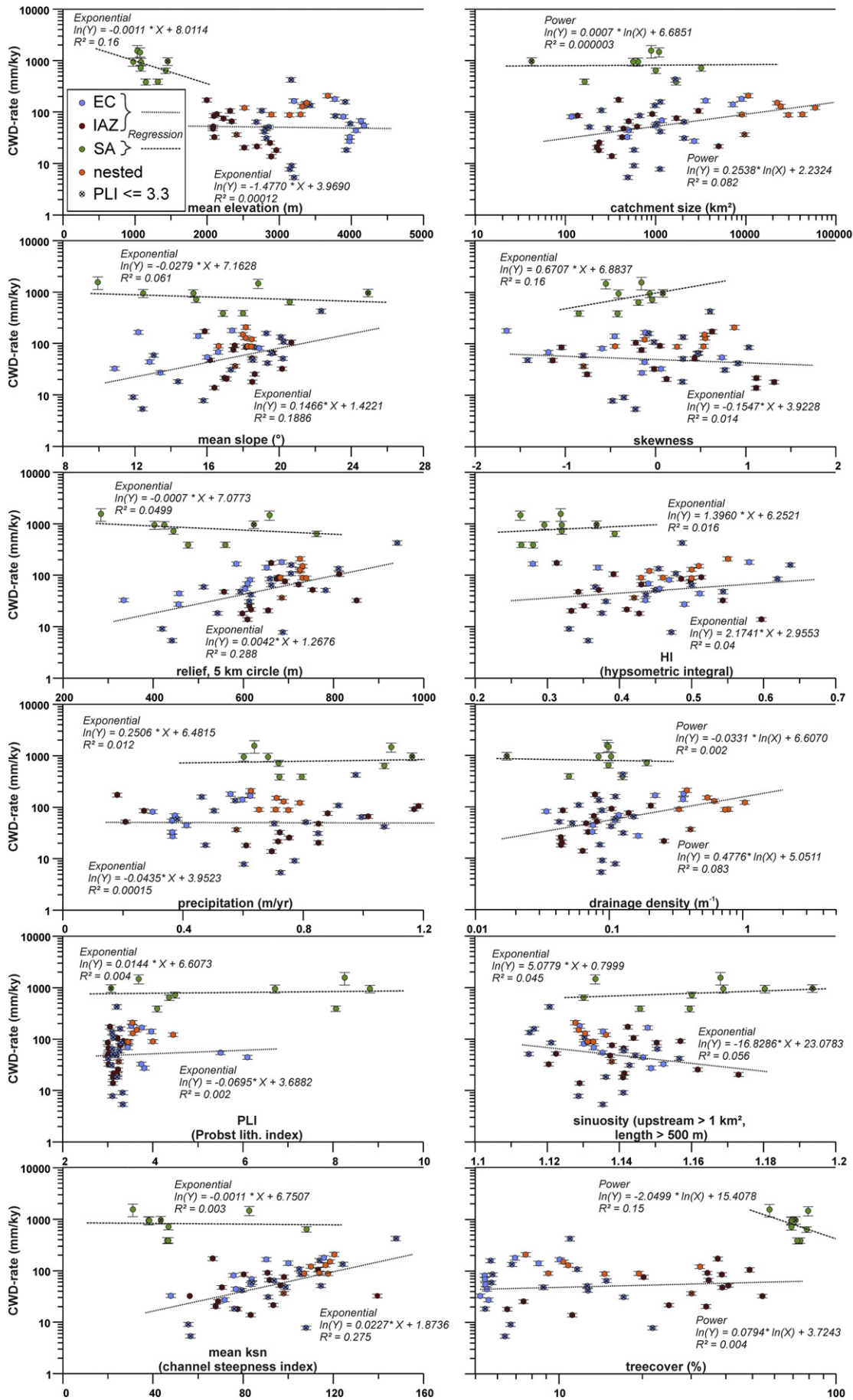
seismic zone in the western part of the EC, whole IAZ and in the western SA. All earthquakes occurring in the EC, between Sucre and Cochabamba, occurred in an area dominated by oblique structures relative to the local deformation front, suggesting transpressive activity dominates there. Thus, we assume that, in our area, earthquakes are structurally defined and that any large, old event occurring west of 64°W was steep and mainly strike-slip (i.e. EC family) in nature, whereas events east of 64°W were of a frontal thrust mode (i.e. SA family, cf. App. 2). We note that recent earthquakes only represent a subset of our dataset, implying that the recurrence time is longer than the observation time. Based on this, we included in our analysis beside the earthquakes listed in App. 2, 30 less constrained events from the CERESIS (2013) catalogue, ranging in magnitude from 5 to 6.4, prior to 1969, and 5 historical earthquakes occurring between 1650 and 1900 (Descotes and Cabre, 1965). In the CERESIS catalogue, local magnitude of recent earthquakes was consistent with the moment magnitudes reported in the Global Centroid Moment Tensor project. Therefore, we derived the seismic moment from an empirical relationship using local magnitude as moment magnitude (Hanks and Kanamori, 1979). Then we computed the uplift for each event as described above, assuming that their dip and rake were the mean values from the relevant earthquake family (App. 2). Thus every event lying in structures parallel and oblique to the range front was considered as frontal thrust or steep transpressive events, respectively. For the CERESIS catalogue data we also computed a range of minimal and maximal cumulative uplift, based on the standard deviation of the rake and dip centroid of strike-slip and dip-slip families (App. 2, Appendix). Note, however, that we assumed a reverse component for all transpressive events whereas some events may have had a normal component leading to an average net subsidence or negative volume (e.g. 22/05/1998 event, App. 2). Therefore the average uplift over long time of these oblique structures is likely closer to their lower bound. This is because we assumed a reverse component for all transpressive events whereas some events may have had a normal component leading to an average net subsidence or negative volume (e.g. 22/05/1998 event, App. 2). As a result, the average uplift over a long time of these oblique structures is likely closer to their lower bound. However, we cannot constrain how often events with a normal component have happened in our historical catalogue. Therefore, if events with normal components are frequent, rock uplift may be significantly impeded, possibly to values close of our post-1969 estimate, whereas if they are rare, the rock uplift will likely remain within our error envelope.

5. Results

5.1. Spatial distribution of denudation rates

Cosmogenic ¹⁰Be denudation rates obtained for 57 catchments range from 5.4 to 1550 mm/ky (Figs. 1–3) (Table 1, Appendix) with a mean value for the Rio Grande of 235 mm/ky (median 85 mm/ky). No catchment size dependency is detected, even though catchment sizes range over three orders of magnitude. The outlet of the studied Rio Grande catchment (RG01, Abapó) yields a rate of 121 mm/ky. Denudation rates in the EC range from 5.4 to 424 mm/ky, with a mean value of 102 mm/ky. An anthropogenically perturbed sample (RG45, gravel works) with a denudation rate of 799 mm/ky is regarded as an outlier and not included in the analysis. In the IAZ, denudation rates range from 13 to 588 mm/ky, with a mean value of 55 mm/ky (ignoring RG14, a comparably small catchment). Samples from the SA yield denudation rates ranging from 390–1550 mm/ky, with a mean value of 892 mm/ky, which is almost ten times higher than the mean rate for the EC and IAZ. Nested samples yield denudation rates between 37 to 208 mm/ky, with a mean value of 113 mm/ky. The effective

Fig. 3. The cosmogenic nuclide derived denudation rates show no or only weak correlation with several geomorphologic parameters metrics (see text for detailed discussion and references). CWD – catchment wide denudation, HI – hypsometric integral, PLI – Probst lithologic index, ksn – channel steepness index.



timescales over which all these denudation rates integrate ranges from 0.4 ky to 111 ky.

The denudation rates show no significant increase downstream even in nested catchments (Fig. 2). While a few single catchments in the EC and IAZ contribute higher denudation rates (outliers RG14, RG39) to an otherwise slowly eroding system, the only marked occurrence of high denudation rates is within the SA. However, this input of material tagged with higher denudation rates does not result in an overall increase in the measured denudation rate at Abapó (RG01). This implies that the higher denudation rates in the SA are currently not perturbing the Rio Grande trunk-stream signal in its lower reaches, which implies that samples are not properly mixed. A test on the validity of this thought can be performed in an area-weighted mixing approach where $D_3 = (D_1 \cdot A_1 + D_2 \cdot A_2) / (A_1 + A_2)$, with D_1 and D_2 the denudation rates in subcatchments with area A_1 and A_2 forming the area of $(A_1 + A_2)$ with denudation rate D_3 . If such a mixing is performed for the Rio Grande catchments between RG15 and RG01 (equal to the physiographic region of the SA only, and “ D_3 ” would equal RG01), the denudation rate at RG01 would be 2–3 times higher than measured. Assuming otherwise, that all sediment at RG01 is just derived from the SA (which in turn requires a SA-specific nuclide production rate for sample RG01), the denudation rate should be only half that of the rate when the entire Rio Grande production rate is considered.

The quartz content within the analysed sediment samples, based on a semi-quantitative estimate during sample processing, varied amongst all physiographic regions. Overall higher quartz contents in the samples from the SA occurred but no clear correlation exists between quartz content and denudation rates. Variations in quartz content were observed elsewhere, revealing no significant bias on denudation rates (Insel et al., 2010; Safran et al., 2005). Therefore, we consider a correction of denudation rates for potential variations in quartz content negligible.

$^{26}\text{Al}/^{10}\text{Be}$ ratios range between 3.5 and 16, whereby samples with a higher ratio than the production rate ratio (>6.5) are almost exclusively samples from the SA. These too high $^{26}\text{Al}/^{10}\text{Be}$ ratios can be explained by the very low measured $^{26}\text{Al}/^{27}\text{Al}$ ratios, which are very sensitive to small variations of the AMS background. We therefore exclude these ratios from further discussion. Samples with $^{26}\text{Al}/^{10}\text{Be}$ ratios distinctly below the steady state production rate ratio are predominantly the nested samples, representing large catchments that are more prone to sediment storage (and hence a faster decay of ^{26}Al compared to ^{10}Be when shielded from cosmic rays). In the following we focus on the ^{10}Be data of non-nested samples in more detail.

5.2. Spatial distribution of topographic parameters and PLI, and their correlation to denudation rates

Our analysis reveals that no single parameter captures the observed denudation rate pattern, i.e., the steep increase in denudation rates from the EC/IAZ to the SA. Local relief (Fig. 3) ranges similarly from 400–1000 m ($D = 5$ km) in each physiographic province (D_5 was chosen with no significant variation when compared with D_3 or D_{10}), mean slopes vary from 10° to 26° and correlate with local relief and k_{sn} but all correlate only poorly with the denudation rate ($R^2 \sim 0.03$ for the whole dataset). The correlation is better when limited to the EC and IAZ but still fairly noisy, with $R^2 = 0.19$. We note that the EC and IAZ have a mostly constant PLI dominated by relatively old and strong rocks contrarily to the SA where the geological units and hence the PLI are very variable with many young and weak Neogene units. It appears that the PLI or rock strength differences throughout our dataset explain most of the scatter. Indeed the catchments with a $\text{PLI} \leq 3.3$ ($n = 30$) are well explained by an exponential function of the slope ($R^2 = 0.61$, Fig. 3), consistent with global relationships (Portenga and Bierman, 2011; Willenbring et al., 2013). On the other hand, the SA catchments have relatively constant high denudation rates for mean slopes ranging

from 9.9° to 24.9° . The mean slope of the SA catchments decreases steadily with increasing PLI, with the lowest slope catchment with PLI about 8, and the catchment with a PLI of 3.3 (RG-10, Figs. 3 and 4). This strongly suggests that mean catchment slope in the SA is modulated by rock strength and explains why very gentle slopes still sustain high denudation rates. When comparing the complete slope probability density function of catchments in the different physiographic regions we find that catchments with high PLI in the SA have very similar modal distributions. Catchments RG-02, RG-06 and RG-08 have a significant part of their catchment covered by valley floors with very low gradients and their modal slope is not relevant for their hillslopes. However, if a mask is applied on the central valley floor of RG-08, we obtain a distribution more relevant to hillslopes and closely matching the other ones with modal values of $\sim 16^\circ$ (Fig. 4). This valley plain signature also explains the shoulder at $\sim 5^\circ$ of RG-04 that contains RG-06 and RG-08. RG-06 and RG-02 have more pervasive Quaternary deposits occupying the plains that are difficult to remove. Tentatively the modal slopes of hillslopes would lie between $12\text{--}15^\circ$, still low but already much higher than modal at $3\text{--}6^\circ$ obtained from the whole catchment. Catchment RG-10, with a similar low PLI to what is mostly found in EC and IAZ (Fig. 4), has the steepest landscape of all catchments, with a modal slope at 27° . In the EC or IAZ the modal slope for individual catchments is between 15° and 20° or lower, with a large diversity of slope distribution shapes (Fig. 4). Though RG-10 is the smallest catchment of our analysis its high slopes are not likely to be a size effect as several other similarly small catchments (RG-32, 41, 55) have much smaller slopes (Fig. 4, Table 1).

Taking into account that the mean slope and the mean elevation (as an input for cosmogenic nuclide production rates for denudation rate estimates) can be compromised by flat areas, that are rather depositional than erosional areas, we performed a sensitivity test by excluding these regions. Considering mean slope, the analysis results in elevated values by a maximum of 4° for catchments with mean slopes less than 18° . It does not change the pattern of correlation between mean slope and denudation or mean slope and PLI. Furthermore, reducing the catchment by the area with low slopes (less than 7°), it results in minor changes in the mean elevation of the respective catchments. Corresponding higher denudation rates of maximum 8% for less than 10% of the catchments are the consequence, with no preferred occasion in the SA. Due to the purely morphometric DEM based analysis and the fact that we ignore geomorphic process regimes, we do not apply such a minor correction.

Furthermore, field evidence and DEM inspection reveal that, in the EC, there is a tendency for steeper slope segments to be predominantly located at the footslope of hillslopes (i.e., the hillslope relief) whereas in the IAZ and SA steeper slopes are more often located at upper hillslopes sections. Slope distributions have no distinct negative skewness for higher modal slopes, which would be indicative of mass-wasting processes and which are commonly associated with higher denudation rates (Wolinsky and Pratson, 2005). The hypsometric integral (HI) (Fig. 3) shows the lowest HI-values in catchments with high denudation rates, suggesting “youthful” or “developing” landscapes for the SA, compared to mature landscapes in the EC and IAZ. Drainage density (D_{dc} and D_{di}) is equally distributed over all physiographic provinces (Fig. 3) and reveals no impact on denudation rates. Mean channel sinuosity for catchments > 1 km² shows little variation, but is tentatively higher in the SA. There, flat valley bottoms dominate and are characterized by the aggradation of point bars and floodplains with riparian vegetation. We infer that a higher sediment flux, assumed by the higher denudation rates, from the lower-order W-E oriented tributaries caused these aggradations and, as a result, higher sinuosities. The channel longitudinal analysis reveals a variable pattern with graded, straight and convex-upward channel segments (Fig. 5). Knickpoints or knickzones occur frequently in the SA and are (i) controlled by lithological changes, (ii) originate when rivers cross anticlines, and (iii) occur when rivers cross thrusts in an oblique fashion. Straight channel sections are

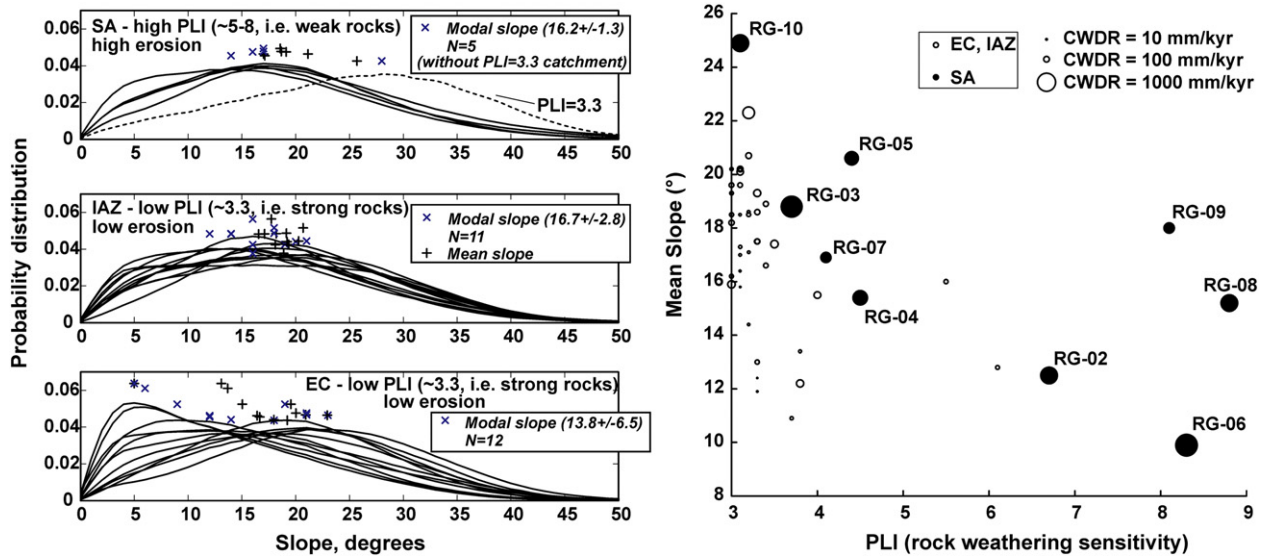


Fig. 4. A) Modal slope distribution of catchments in the individual physiographic regions. B) Mean slopes plotted against PLI with circles indicating the relative magnitude of denudation rates.

commonly parallel to the strike of major faults and alignment of major valleys. No strong control of the channel longitudinal river channel profile from denudation rates could be detected (Fig. 5).

The orientation of major structural trends and the predominant orientation of topographic highs and lows, including fluvial channels, show a two-fold pattern (Fig. 6). The overall structural trend is controlled by the Bolivian orocline, where a predominant NW-SE trend turns into an N-S trend at ~18°S (Fig. 1 inset). While the structural trend in the EC and IAZ is predominately NW-SE with a uniform distribution of fluvial drainages, it changes into a distinct N-S orientation with a pronounced E-W orientation of tributary trellis drainage patterns and a strike-parallel orientation of the trunk-stream in the SA. The only weakly preferred orientation of drainages in the EC and IAZ suggests a balance between structural control and drainage occupation and higher

maturity of the landscape. In contrast, the distinct pattern of drainages oblique to the structural grain in the SA highlights the E-W alignment of tributaries and suggests a tectonic control on drainage orientation. However, none of the outlined characteristics seems to represent a prime control factor for the observed denudation rates.

We have highlighted a combined control of slope and lithology on the denudation rate across the different physiographic region. Although slopes are mostly gentle in the SA, the catchments seem to be forced into a steep state relatively to their rock strength. The very steep slopes and high denudation rate of the RG-10 catchment, with a strong lithology equivalent to the ones of the IAZ and EC, confirm that an external process must support and steepen the landscape in the SA, and that we are not detecting the transient removal (i.e., denudation) of the very weak frontal layers.

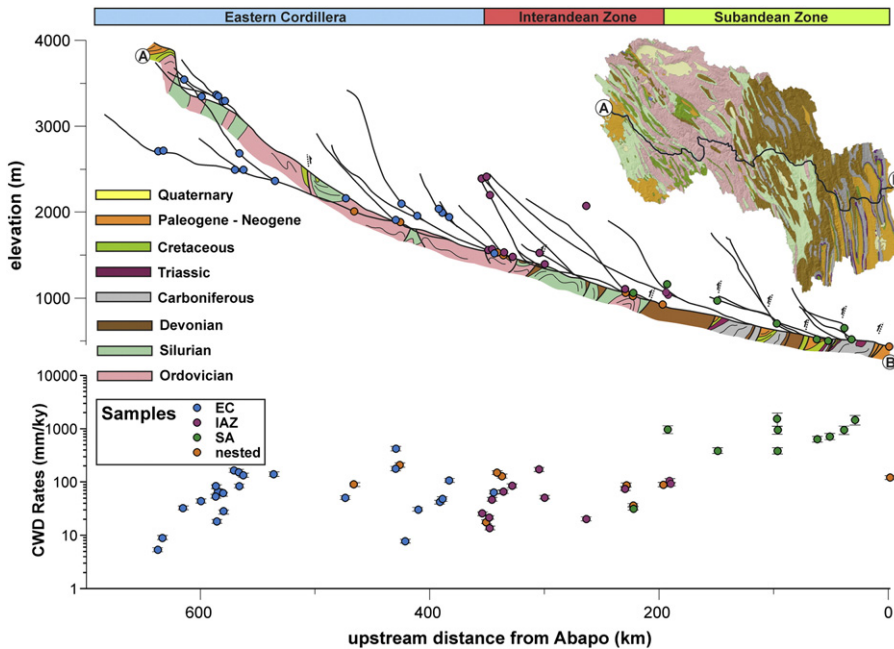


Fig. 5. River length profiles of the major Rivers in the upper Rio Grande catchment. Profiles were extracted from Aster GDEM data (30 m resolution) and intersected with the sample locations, major structures, and the geology (for trunk stream segment).

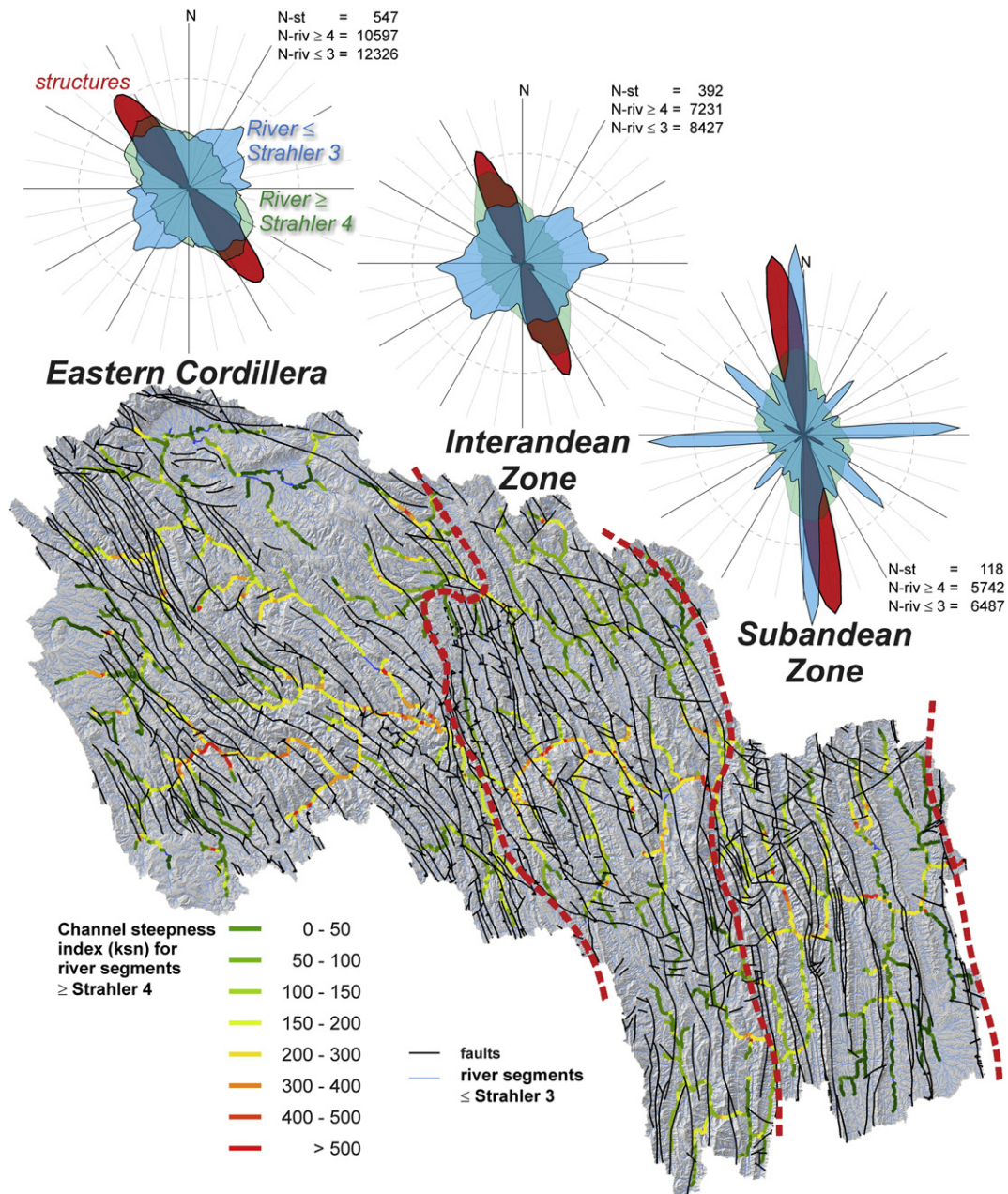


Fig. 6. Orientation of fluvial network and tectonic structures presented as rose diagrams (see text). The fluvial network is homogeneously distributed in the EC. Towards the SA, it is closely associated with the structural grain and implies an active tectonic control. The extreme peaks for the directions of rivers smaller than Strahler order 3 in the SA are artifacts of the river extraction method. Even reducing the peaks by half would still show the two main directions, along and perpendicular to the structures. The channel steepness index map for river segments higher than Strahler order 3 do not indicate larger differences between the Eastern Cordillera, the Interandean Zone and the Subandean Zone.

5.3. Tectonics and seismicity

The seismic analysis of recent and historical shallow earthquakes shows a two-fold pattern with higher seismically uplifted volume in the SA correlating with the order of magnitude higher denudation rates obtained in this study and vice versa, lower uplifted volumes and lower denudation rates in the EC and IAZ (Fig. 7). Based on measured and interpolated historic events, the cumulative seismic moments (and thus likely peak ground accelerations, PGA) of the Cochabamba and SA regions are essentially similar in magnitude, but slightly larger in the Cochabamba region. However, the seismic moment release in the Cochabamba region is associated with a much lower cumulative seismic uplifted volume due to the strike slip dominance

(two orders of magnitude over the past 40 years; Fig. 7). Historical data over the past 400 years show a persistent seismicity in the eastern Andes and suggest a higher cumulative uplifted volume in the SA (3.5 to 30 times larger). We lack observations on possible aseismic or interseismic sources of uplift and will address this issue in the discussion. We rule out deeper uplift sources (isostasy or dynamic topography), which seem unlikely to have such variations at these small spatial scales (<100 km) and are negligible for the Rio Grande region on late Cenozoic timescales (Dávila and Lithgow-Bertelloni, 2013). Note that the established, seismicity based, volume uplift estimates are on a similar timescale compared to the cosmogenic nuclide derived estimates for denudation rates in the SA, i.e. integrated over a few hundred years.

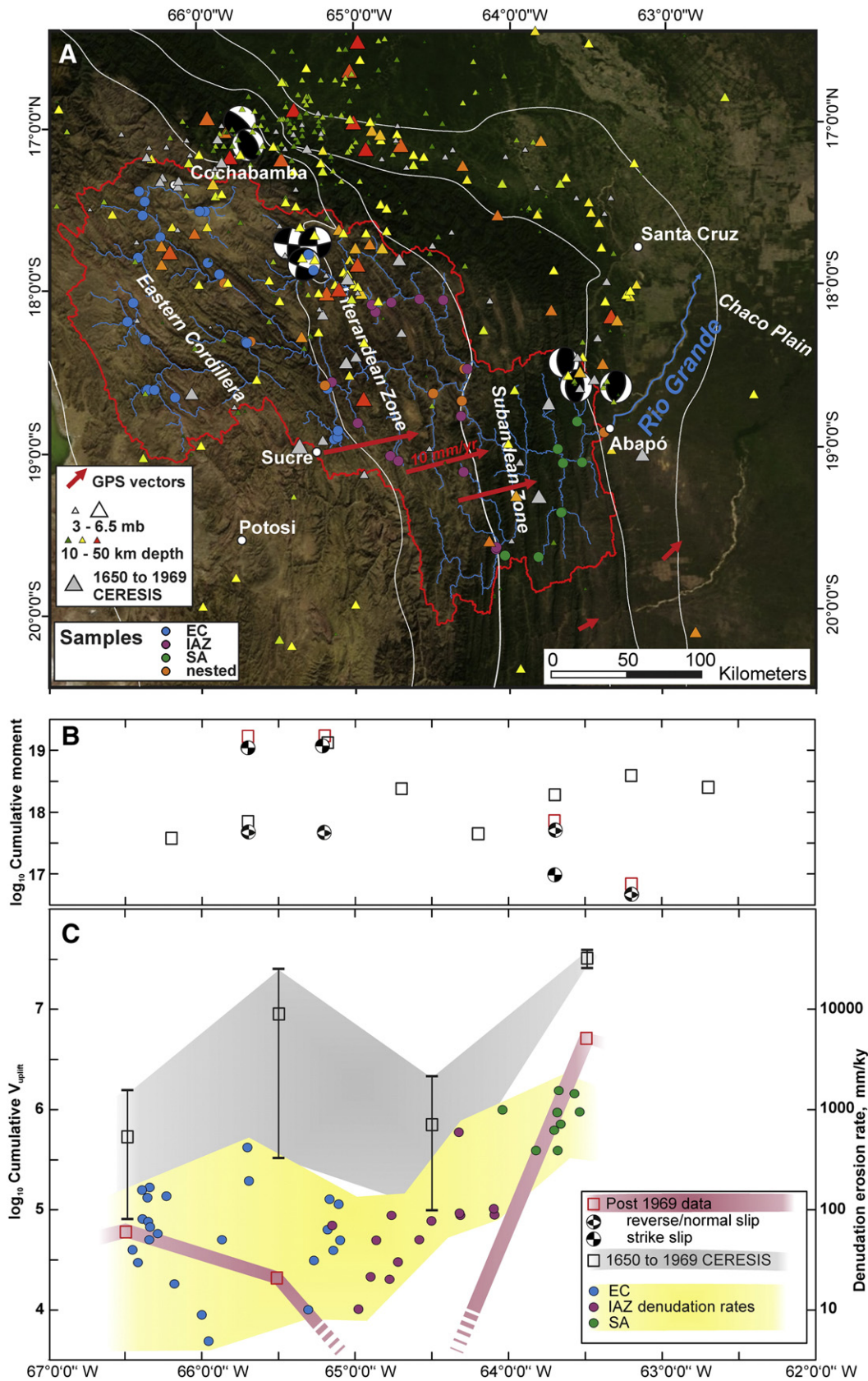


Fig. 7. (A) Seismicity, fault plane solutions (<http://www.isc.ac.uk>), and GPS velocity field (red arrows, Brooks et al., 2011) in the Rio Grande catchment vicinity. Shown are also color coded sample locations. (B) Cumulative seismic moment (log scale) with indicated mode for post 1969 earthquakes based on the GCMT (Dziewonski et al., 1981; Ekström et al., 2012) and Vega and Buforn, 1991) and the CERESIS (2013) Catalogue for historic ones. (C) Calculated seismically uplifted volume (see text) with an uncertainty envelope. Note that more measured earthquakes occurred at and with lower uplifted volume. Calculations for historic earthquakes are based on modern ones (see text). Both seismic datasets show higher uplift in the SA, corresponding to higher denudation rates (note log scale).

5.4. Climate, vegetation and denudation rates

Although mean precipitation rates and denudation rates both decrease towards elevations above 3000 m, the pronounced spatial variation of denudation rates do not correlate with the spatial distribution of the annual precipitation pattern (Figs. 1 and 3). Similarly, vegetation coverage is highest in the low-lying and faster eroding SA, while the more slowly eroding IAZ and EC are more sparsely vegetated, but again, no clear pattern to the prevalent pattern of low and high denudation rates is detectable.

5.5. Centennial sediment yield derived denudation rates

There is a marked difference between millennial, cosmogenic denudation rates and modern sediment yield rates (Fig. 8). Modern sediment yield derived denudation rates (revised by Aalto et al., 2006, and Pepin et al., 2013; based on earlier data by Guyot et al., 1994, 1996) imply outlet denudation rates at Abapo of 930–980 mm/ky, which are nine times higher than those obtained by the cosmogenic nuclides in this study, and two times higher than rates reported by Wittmann et al. (2009). Sediment yield data for the EC and IAZ range from 190–4640 (median = 1040 mm/ky) which is again up to an order of magnitude greater than the values obtained by cosmogenic nuclides. However, adjacent catchments southward of the Rio Grande yielded lower sediment yield values, equivalent to rates between 260–710 mm/ky (samples AT, NU, VQ, in Aalto et al., 2006). This argues for episodic events being recorded by the sediment yield data for the Rio Grande catchment, as already discussed by Guyot et al. (1994).

6. Discussion

A transect across the central Bolivian Eastern Andes reveals that low denudation rates characterize catchments from the EC and IAZ (mean ~100 mm/kyr), while denudation rates in the SA are up to an order of magnitude higher (mean ~800 mm/kyr). This signature is not related to a single quantitative geomorphic parameter. In the absence of a significant climate control, we link the observed denudation rate pattern to tectonic forcing and rock strength properties. In the following, we will first outline the seismic control on landscape evolution and denudation rates, before arguing on the lithologically controlled threshold conditions of classical geomorphic parameters and the resulting transience of the landscape.

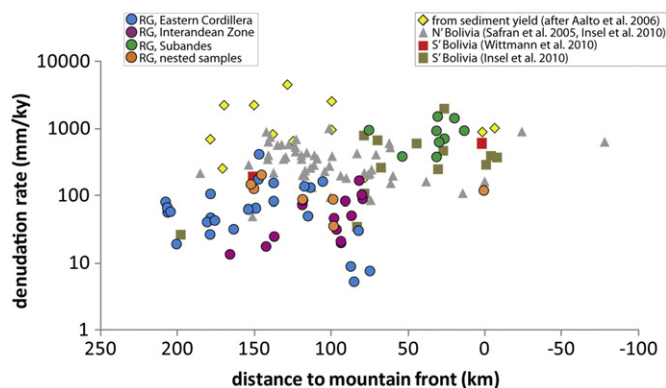


Fig. 8. Compilation of denudation rates for the Rio Grande (this study) and regional data from Insel et al. (2010) for the Rio Grande region. Data from the Subandes east of the more active Eastern Andes at the La Paz latitude are similar to the ones from Safran et al. (2005). Also shown are selected data from Wittmann et al., 2011). Sediment yield from Aalto et al. (2006, see text) are converted to denudation rates (density 2.5 g/cm⁻³). Some samples within the EC have a smaller distance to the mountain front in the NE than IAZ samples to the mountain front in the E.

6.1. Denudation rates, tectonic forcing, rock strength and missing topographic signatures

An analysis of the cumulative seismic moment based on recent and historical earthquakes for the eastern Bolivian Andes suggests slightly higher values in the Cochabamba region (EC) compared to the SA. While cumulative seismic moment cannot explain the variations in denudation rates between both regions, we relate it to the seismically uplifted volume (i.e., building of topography; Fig. 7), which is higher in the SA region due to the thrust mode. While the earthquake data are scarce and therefore the uplift data is at a very coarse spatial scale, we can only suggest with our analysis that along the front, historical earthquakes produce an order of magnitude more rock uplift than the transpressive ones in Cochabamba area. However they have a similar total moment. At the first order we also observe a fairly constant denudation rate in the SA, which are one to two orders of magnitude higher than in the EC/IAZ. Therefore, we cannot easily quantify an explanatory power for the uplift pattern. Nevertheless, relating uplift and denudation is supported by the following facts: (i) the focus of active deformation is currently in the SA and corresponds with the current orogenic front propagating into the Chaco Plain (Horton, 1999; Oncken et al., 2012), (ii) young deformation ages and high exhumation rates in the SA (Barnes et al., 2012; Oncken et al., 2012), and (iii) geodetic data, paleomagnetic data and subsurface faulting evidence which yields highest differential uplift in the SA (Brooks et al., 2011; Dimate et al., 1999; Lamb, 2000). Other parameters that suggest ongoing tectonic activity in the SA are concave upward river profiles, knickzones and higher channel sinuosities. Furthermore, low hypsometric integrals reflect a tectonically induced rejuvenation of the landscape and the ongoing construction of topography (Ohmori, 1993) (Fig. 3). Contrary to other studies, e.g. in the Himalaya, where clear correlations exists between rock uplift, channel steepness and denudation rates (Scherler et al., 2014), the situation in the Rio Grande seems to inhomogeneous in terms of lithology and/or too less sensitive in terms of climate to provide such correlations.

Since a few decades it has been observed that, in tectonically active landscapes, denudation rates can vary widely over an area with constant mean slopes (e.g. Burbank et al., 1996). Such landscapes are referred to as threshold landscapes where bulk hillslope mechanical strength limits the topographic gradient and decouples it from the denudation rate (Burbank et al., 1996; Montgomery and Brandon, 2002; Ouimet et al., 2009; Schmidt and Montgomery, 1995). In those areas, where the topography reaches its threshold slope, any additional uplift leads to river incision and associated mass wasting is required to retrieve a gradient below the threshold. This theory has been confirmed in areas where the rate of landsliding, and therefore denudation rate, correlates with the uplift rate and the river incision rate (Korup, 2008; Larsen and Montgomery, 2012). Similarly, the slope distribution and especially its modal are thought to be a proxy for the bulk hillslope rock strength (Korup, 2008; Korup and Weidinger, 2011). Thus it is tempting to interpret our observations as characteristics of a threshold landscape. The higher relative uplift located close to the deformation front may have forced the topography to its threshold state, leading to uniform slope distribution with a modal slope of ~17° for catchments dominated by high PLI (4–8, weaker rocks), and to modal slope of 27° for low PLI (<3.3, stronger rocks). Hence, the higher uplift rate inferred from our seismic analyses and from geodynamical studies (see above) would be responsible for the 5–10 fold higher denudation rates in the SA.

However, several puzzling observations need to be considered. First, the main denudation process in threshold landscapes has been recognised as bedrock landsliding (Burbank et al., 1996; DiBiase et al., 2010; Korup, 2008) that is rarely observed in the Subandes, both in the field and on aerial imagery. Second, typical threshold landscapes have modal slopes between 30° and 35° when measured on coarse (30–90 m) DEMs (Burbank et al., 1996; Korup, 2008), whereas we

propose a threshold landscape with modal slopes as low as 17°. A first interpretation would be that the landscape is close to but not yet at its threshold. In this case, the relief and slope would be close enough to their critical value to explain relatively high denudation rates due to soil creep and gullyng (cf Roering et al., 2007), but uplift would also steepen the landscape. Therefore, the topography would be in a transient state, with a critical slope larger than the current modal slopes and active landsliding would be expected to turn on at the end of this growing phase, relatively soon compared to the landscape age. The resolution of the existing spatial uplift information (Lamb, 2000) precludes any further investigation here.

On the other hand, catchment RG-10 has a modal slope of 27°, similar to what was observed in weak Himalayan lithologies (Korup and Weidinger, 2011), and the lithological strength of most of the Subandes may well be significantly weaker than the lithology of the previously identified threshold landscape. Then, landsliding may be the dominant erosion process. It is currently unclear, why landslides occur only with limited spatial extent in the field (evidenced in occasional shallow landslides and soil slips in the field) or are incompletely detected on aerial imagery (Lee, 2013). Nevertheless, the impact on denudation and sediment fluxes of isolated landslides can be temporally and spatially large (Blodgett and Isacks, 2007; Coppus and Imeson, 2002). It has also been observed that earthquake triggered landslides occur preferentially close to ridges, and may not directly supply sediment to streams (Meunier et al., 2008) and are thus not to be observed near streams during field studies. Material released upslopes by this process will eventually be transported into trunk streams, with a delayed response (probably within the ^{10}Be integration time scale). With a relatively small uplift component forcing denudation it may be possible that high magnitude low frequency landslide events, possibly due to large and rare earthquakes (e.g. Brooks et al., 2011) or exceptional climatic pulses steer denudation. Such past events must be recent enough to have been captured within the ^{10}Be integrated signal (~500 yr) and also be old enough to have allowed vegetation to fully re-establish, implying centennial timescales. Paleoseismic studies or geomorphologic evidences of old large landslide may help to confirm such hypothesis.

Alternatively, another process may be coping with the relatively small uplift and maintaining the topography at its threshold angle and thereby controlling catchment denudation. Although less efficient than landsliding, we speculate that earth-flows and non-linear soil diffusion could be the predominant erosional processes (Roering et al., 2007). Earthflows typically occur at slopes of 15–20° (Mackey and Roering, 2011; Scheingross et al., 2013) and have been shown to be responsible for up to 0.5 mm/yr of catchment average denudation rates (Mackey and Roering, 2011). A few active earthflows could be responsible for half or more of the total denudation, the rest being likely due to other soil processes and gullyng (Booth and Roering, 2011). This scenario seems especially consistent with the highly weatherable lithologies and the dense tree cover that would yield a relatively thick soil cover and increase the likelihood of earthflows. Earthflows could have been missed because they are less conspicuous than landslides scars as they do not fully clear vegetation, making them much harder to detect from aerial imagery. Hence, since we currently lack direct observation additional field surveys would be required in order to assess a possible control of earthflows on the denudation budget of the Subandes.

Besides rock strength, field observations do not support a major contribution of fracture density on denudation rates, although such a positive dependency could be expected in a fold and thrust belt (Flores-Niño et al., 2005; Molnar et al., 2007). It could be even enforced by earthquake induced bedrock-fracturing and weakening (Hovius et al., 2011), however such an impact was not further explored here.

So far we have left open the issue of aseismic and interseismic deformation. Insights on this can be gained from geodetic observations. Recently, GPS-shortening rates have been updated to 9–13 mm/yr near Sucre and south of the Rio Grande catchment (Brooks et al., 2011)

consistent with Quaternary shortening based on cross-sections (7–10 mm/yr) (Echavarría et al., 2003). The shortening pattern indicates a fully locked, 100 km wide, subhorizontal detachment that does not support aseismic slip in the SA and suggests a negligible component of interseismic uplift at the front. However, further to the west the detachment is likely slightly steeper, i.e. up to 5°, and may yield up to 0.5–1 mm/yr of uplift below the EC, west of Sucre. Yet, this GPS dataset excludes the area of oblique structures that occupies most of the IAZ and EC at the latitude of the Rio Grande. Therefore, it does not account for an increase in the strike slip component of shortening and a likely different geometry that may reduce this uplift rate. Nevertheless, Brooks et al. (2011) also suggested that large magnitude (Mw 7.5–8.9) earthquakes would rupture the most frontal thrust, with recurrence time of ~500–1500 years. They also suggest that, at least to the South, neotectonic activity seems to be focused at the very front. Such large earthquakes would certainly result in significant uplift over the entire width of the SA, contrarily to the historical earthquakes that we have compiled, that are insufficient to reach a homogeneous uplift rate of ~1–2 mm/yr over the whole SA (Lamb, 2000). Therefore it seems reasonable that our observed differential uplift would be reinforced by larger, older earthquakes that are not included, and not counterbalanced by significant aseismic or interseismic uplift.

6.2. Climatic control on denudation rates and sediment routing

The denudation rate pattern obtained for the Rio Grande does not show a strong correlation with precipitation and exhibits only a weak dependence with climate variability (Seiler et al., 2013, Fig. 9). Rainfall is similarly high in the SA and IAZ, and even in parts of the EC (Fig. 1). Tree cover does decrease from the SA to the EC, and mainly correlates with elevation (Fig. 3). One could suspect that the dense vegetation of the SA would protect the landscape and would cause low erosion rates in the SA (Vanacker et al., 2007). While this corresponds with the field evidence of limited mass wasting events, it does not correspond with the high denudation rates observed in the SA. However, such events may be reflected in the exceptionally high intramountain short-term sediment gauged rates reported by Guyot et al. (1994). In summary, although climate and its variability via precipitation, runoff and vegetation may affect denudation processes (Istanbulluoglu and Bras, 2006), their actual contribution to the magnitude of denudation rates in the Rio Grande remains elusive and is probably of second order, as has been suggested elsewhere (Bermúdez et al., 2012; Godard et al., 2014; Kirchner et al., 2001; Riebe et al., 2001; Scherler et al., 2014).

Commonly, the integration periods of cosmogenic nuclide derived catchment wide denudation rates are on the order of 10^2 – 10^4 yr. Therefore they are more prone to respond to climate variations than to regional scale tectonic perturbations. As suggested by Insel et al. (2010) for the SA, Holocene climate variations may have set the cosmogenically derived denudation rates out of equilibrium. Such climate variations would have likely influenced the EC and IAZ similarly, for which we have no indications. Assuming such scenarios, landslides or debris flows could have activated due to changes in magnitudes or frequency of precipitation, or due to higher levels of water saturation of soils or modified groundwater pathways. However, we have no clear indications for a primary climatic control on denudation rates as outlined above.

6.3. Cosmogenic nuclide mixing in time and space

Ten years prior to our study, Wittmann et al. (2009) analysed several samples which were collected closely to our nested samples. For one sample from the EC (RG27 vs. GR25), identical denudation rates within uncertainties were obtained. For another comparable set of samples at Abapò (RG01 vs. GR19), however, our measurement yielded a 5 times lower model value. The latter variation is large when compared to

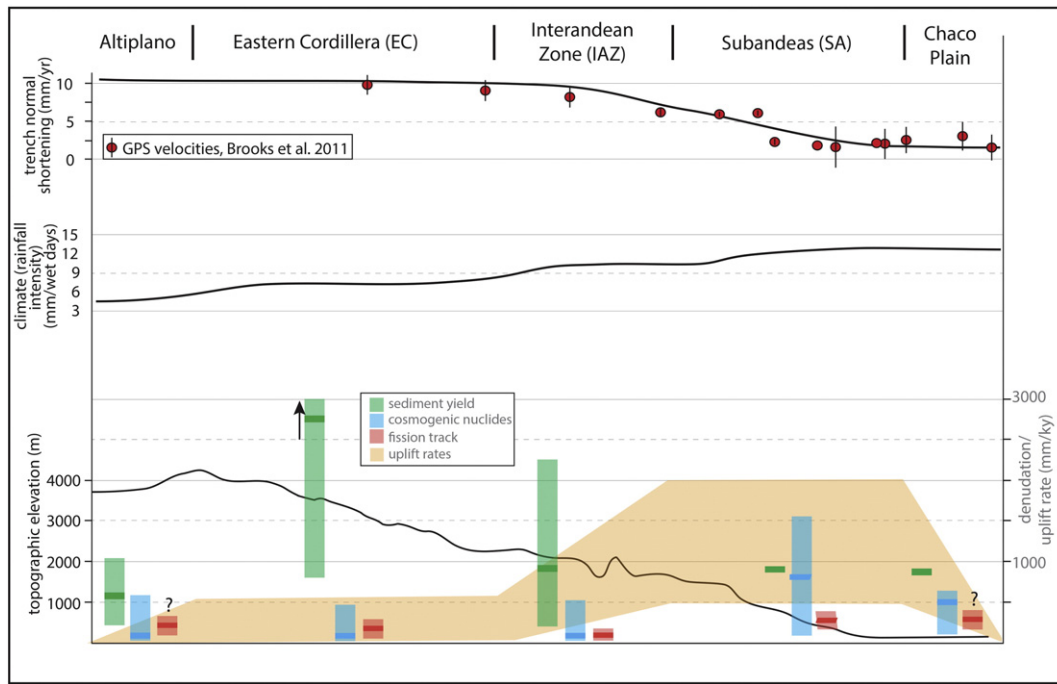


Fig. 9. Summary of uplift rates (Lamb, 2000) and denudation rates for decadal (sediment yield, Aalto et al., 2006), millennial (this study, Hippe et al., 2012 for the Altiplano) and fission track data (Barnes et al., 2012). While short decadal rates are likely associated with episodic events and approach extraordinary high values (EC and SA), the general the pattern of cosmogenically derived denudation rates follows closely the uplift. Shortening is according to Brooks et al. (2011). Climate pattern (here shown as rainfall intensity [mm (wet days)⁻¹] after Seiler et al. (2013).

other studies, e.g., in the Himalayas, where ¹⁰Be denudation rates varied by no more than a factor of two in similarly large catchments, for samples obtained during repeated sampling campaigns (Godard et al., 2012; Lupker et al., 2012) or in smaller alpine catchments dominated by debris-flows (Kober et al., 2012). Our preferred interpretation for the discrepancy observed here is that the cosmogenic nuclide concentration measured in sample RG01 preserves a signal from the EC/IAZ headwaters with only minor admixture of material from the faster eroding SA (i.e., the SA is under-represented in our samples). In contrast, local activation of SA-derived material tagged with high denudation rates may be over-represented in the samples analysed by Wittmann et al. (2009). The latter fact is supported by the agreement in data from samples further upstream (RG27 vs. GR25), which signifies that episodic events in the EC and IAZ are difficult to trace, also with cosmogenic nuclides (Yanites et al., 2009). This highlights that even repeated measurements of cosmogenics nuclides may not pick up adequately episodic events, where either hillslope processes or sediment source-to-sink dynamics are not adequately represented in a sample.

The detection of intermittent storage of sediment in the routing system can be quantified with a multiple nuclide approach (Kober et al., 2009). Larger regions are containing more terrace and floodplain areas with limited sediment connectivity forcing sediment storage. The lower ²⁶Al/¹⁰Be ratios for the nested samples suggest that in the larger catchments intermittent storage could occur. In contrast, the higher sinuosity and associated potential to store sediment in the SA, is not reflected in the ²⁶Al/¹⁰Be ratios, suggesting, that these areas are not sufficiently large and storage times too short. However, we acknowledge, that the detection of such variation is hampered by the low nuclide concentrations measured in the SA. Storage of sediment on the order of a few (~3) ky was suggested for the Andes (Dosseto et al., 2006) but is, according to our data, more on the order of 10⁶ yrs. Complex nuclide ratios were observed earlier (Insel et al., 2010; Safran et al., 2005; Wittmann et al., 2009) and certainly need a more thorough investigation which is out of the scope of this paper.

6.4. Regional Comparison

On the Rio Grande latitude, climate and its variability play only a secondary role in landscape evolution on the Eastern Andean flank. However, the dry regions of the Altiplano or Western Escarpment farther to the west show a clear regional denudation rate dependency on the climatic regime (Figs. 8 & 9; Hippe et al., 2012; Kober et al., 2009). Those might be in a steady state with the prevailing, though less active, tectonic regime, however, acting on much longer integration timescales of landscape processes and nuclide systematics. Along strike of the Eastern central Andes, the climate influence is more pronounced (Hilley and Coutand, 2009; Montgomery et al., 2001). Similarly, denudation rates at comparable latitudes at the western flank of the Andes may be affected by climate variability such in very arid areas and have rather denudation rates that anti-correlate with precipitation (Carretier et al., 2013). Studies in the La Paz region/latitude revealed orographic rainfall and higher climate variability resulting in higher denudation rates in the EC (Fig. 8) (Barnes et al., 2012; Insel et al., 2010; Safran et al., 2005). As a result climatically focused erosion concentrates the tectonic activity in a narrow zone consistent with critical wedge theories (Horton, 1999). The interplay between tectonic and erosion is additionally modulated by deep river dissection (Zeilinger et al., 2010; Zeilinger and Schlunegger, 2007), where geomorphic indices partially trace the magnitude of denudation rates (Safran et al., 2005). Such effects are not obvious for the eastern Andes in the Rio Grande region.

7. Conclusion

An across strike transect of denudation rates in space and time of the upper Rio Grande reveals that denudation rates over short and long-timescales are highest in the SA since the Late Miocene/Pliocene (Fig. 9). The denudation rate pattern correlates with the tectonically induced uplift pattern in the region, the uplift being most active in the SA. Additionally, higher denudation rates are associated with lower

rock-strength lithologies in the SA compared to the EC and IAZ. This results in geomorphic indices in the EC, IAZ and SA that are less distinct than one could expect for such a tectonically active setting.

We argue that the formation of topography in the SA – incipient in Late Miocene/Pliocene to recent times – causes higher denudation rates in an actively migrating fold and thrust belt. Seemingly, the denudation rates are sufficiently high to impede construction of a higher topography or already balancing any further construction. Keeping in mind that tectonic and denudation rates are spatially and temporally transgressive in a mountain belt evolution with growing, steady and waning phases of topography (Montgomery, 2001) it remains ambiguous to derive general conclusions. We suggest that in the SA the growing phase of topography is transient and close or already at its threshold limit, respectively. This transient topography, where denudation is balancing tectonic uplift, is however controlled by a tectonic forcing which may be stagnant or strain accumulating (Brooks et al., 2011) or just not fully detectable on recent and historical timescales (by e.g., earthquakes).

We conclude that the overall denudation rate signature of the central eastern Andes seems to be controlled primarily by tectonic uplift, with an important modulation due to lithologies and associated rock strength, causing a complex pattern of geomorphic processes and responses. In contrast to other studies, the relatively high denudation rates are not always associated with high relief and steep slopes or topographies which are commonly observed in tectonically active regions. Overall, it is also likely an effect of the nonlinearities in landscape response and reaction timescales to climate or tectonic perturbation as well as variable threshold conditions for sediment transport (Istanbulluoglu and Bras, 2006).

We identify potential in more detailed investigations of seismic movements and uplift and its relation to denudation rates in order to understand the complex interplay between tectonic, climate, denudation and regional geological inheritance (e.g., rock properties, fracture pattern). Furthermore, understanding the effects of landsliding and earthflow activity in various lithologies causing low to intermediated threshold slopes needs further exploration.

Acknowledgements

This research was funded by the Viceministerio de Recursos Hídricos y Riego (VRHR) and the Apoyo Sectorial Plan Nacional de Cuencas (ASPNC) in collaboration with GIZ. We thank Carlos Ortuño Yañez and Sohrab Tawackoli for their support. The project benefited from discussions with Has Willett. The sampling campaign also benefited from the efforts by the drivers Thomas and Augusto, and field assistants Jomaha, Jamila and Vanessa. O. Marc is funded by a fellowship in the EU Marie Curie International Training Network TOPOMOD, project reference number 264517. We acknowledge the help of UP-Transfer in administration issues. Input by and discussions with Niels Hovius and Cassandra Fenton in the later stage of the project sharpened the interpretation presented here. The thorough reviews by D. Scherler and an anonymous reviewer are acknowledged.

F. Kober and G. Zeilinger contributed equally to this manuscript.

Appendix A. Supplementary data

Supplementary data to this article can be found online at <http://dx.doi.org/10.1016/j.tecto.2015.06.037>.

References

- Aalto, R., Dunne, T., Guyot, J.L., 2006. *Geomorphic Controls on Andean Denudation Rates*. *J. Geol.* 114, 85–99.
- Balco, G., Stone, J.O., Lifton, N.A., Dunai, T.J., 2008. A complete and easily accessible means of calculating surface exposure ages or erosion rates from Be-10 and Al-26 measurements. *Quat. Geochronol.* 3 (3), 174–195.
- Barnes, J.B., Ehlers, T.A., McQuarrie, N., O'Sullivan, P.B., Tawackoli, S., 2008. Thermochronometer record of central Andean plateau growth, Bolivia (19.5 degrees S). *Tectonics* 27 (3).
- Barnes, J.B., Ehlers, T.A., Insel, N., McQuarrie, N., Poulsen, C.J., 2012. Linking orography, climate, and exhumation across the central Andes. *Geology* 40 (12), 1135–1138.
- Bermúdez, M.A., van der Beek, P.A., Bernet, M., 2012. Strong tectonic and weak climatic control on exhumation rates in the Venezuelan Andes. *Lithosphere* 5, 3–16.
- Blodgett, T.A., Isacks, B.L., 2007. Landslide Erosion Rate in the Eastern Cordillera of Northern Bolivia. *Earth Interact.* 11 (19), 1–30.
- Bookhagen, B., Strecker, M.R., 2008. Orographic barriers, high-resolution TRMM rainfall, and relief variations along the eastern Andes. *Geophys. Res. Lett.* 35.
- Bookhagen, B., Strecker, M.R., 2012. Spatiotemporal trends in erosion rates across a pronounced rainfall gradient: examples from the southern Central Andes. *Earth Planet. Sci. Lett.* 327–328, 97e110.
- Booth, A.M., Roering, J.J., 2011. A 1-D mechanistic model for the evolution of earthflow-prone hillslopes. *J. Geophys. Res.* 116, F04021. <http://dx.doi.org/10.1029/2011JF002024>.
- Brooks, B.A., et al., 2011. Orogenic-wedge deformation and potential for great earthquakes in the central Andean backarc. *Nat. Geosci.* 4 (6), 380–383.
- Burbank, D.W., 2002. Rates of erosion and their implications for exhumation. *Mineral. Mag.* 66, 25–52. <http://dx.doi.org/10.1180/0026461026610014>.
- Burbank, D.W., Anderson, R.S., 2001. *Tectonic Geomorphology*. Blackwell, Malden, MA, p. 274.
- Burbank, D.W., Leland, J., Fielding, E., Anderson, R.S., Brozovic, N., Reid, M.R., Duncan, C., 1996. Bedrock incision, rock uplift and threshold hillslopes in the northwestern Himalayas. *Nature* 379, 505–510.
- Carretier, S., et al., 2013. Slope and climate variability control of erosion in the Andes of central Chile. *Geology* 41, 195–198.
- Champagnac, J.-D., Molnar, P., Sue, C., Herman, F., 2012. Tectonics, climate, and mountain topography. *J. Geophys. Res. Solid Earth* 117 (B2), B02403.
- Chmieleff, J., von Blanckenburg, F., Kossert, K., Jakob, D., 2010. Determination of the Be-10 half-life by multicollector ICP-MS and liquid scintillation counting. *Nucl. Instrum. Methods Phys. Res., Sect. B* 268 (2), 192–199.
- Christl, M., et al., 2013. The ETH Zurich AMS facilities: Performance parameters and reference materials. *Nucl. Instrum. Methods Phys. Res., Sect. B* 294, 29–38.
- Codilean, A.T., 2006. Calculation of the cosmogenic nuclide production topographic shielding scaling factor for large areas using DEMs. *Earth Surf. Process. Landf.* 31 (6), 785–794.
- Coppus, R., 2002. *Landscape sensitivity to erosion in three semi-arid Central Andean ecosystems*. University of Amsterdam, Amsterdam (147 pp.).
- Coppus, R., Imeson, A.C., 2002. Extreme events controlling erosion and sediment transport in a semi-arid sub-andean valley. *Earth Surf. Process. Landf.* 27 (13), 1365–1375.
- Dadson, S.J., et al., 2003. Links between erosion, runoff variability and seismicity in the Taiwan orogen. *Nature* 426, 648–651.
- Dávila, F.M., Lithgow-Bertelloni, C., 2013. Dynamic topography in South America. *J. S. Am. Earth Sci.* 43, 127–144.
- De Fries, R.S., Hansen, M., Townshend, J.R.G., Sohlberg, R., 1998. Global land cover classifications at 8 km spatial resolution: the use of training data derived from Landsat imagery in decision tree classifiers. *Int. J. Remote Sens.* 19 (16), 3141–3168.
- Defries, R.S., Hansen, M.C., Townshend, J.R.G., Janetos, A.C., Loveland, T.R., 2000. A new global 1-km dataset of percentage tree cover derived from remote sensing. *Glob. Chang. Biol.* 6 (2), 247–254.
- Descotes, P.M., Cabre, R., 1965. *Historia Sismica de Bolivia*. Bol. Inst. Boliviano del Petreo 5, 16–28.
- Díaz, H., et al., 2010. Caracterización de la cuenca de la cuenca Alta del río Grande y el Chaco Cruceño, Santa Cruz, Bolivia.
- DiBiase, R.A., Whipple, K.X., Heimsath, A.M., Ouimet, W.B., 2010. Landscape form and millennial erosion rates in the San Gabriel Mountains, CA. *Earth Planet. Sci. Lett.* 289 (1–2), 134–144.
- DiBiase, R.A., Heimsath, A.M., Whipple, K.X., 2012. Hillslope response to tectonic forcing in threshold landscapes. *Earth Surf. Process. Landf.* 37 (8), 855–865.
- Dimate, C., et al., 1999. Seismic hazard assessment in the Northern Andes (PILOTO Project). *Ann. Geofis.* 42 (6), 1039–1055.
- Dosseto, A., Bourdon, B., Gaillardet, J., Maurice-Bourgoin, L., Allegre, C.J., 2006. Weathering and transport of sediments in the Bolivian Andes: Time constraints from uranium-series isotopes. *Earth Planet. Sci. Lett.* 248 (3–4), 759–771.
- Duvall, A., Kirby, E., Burbank, D., 2004. Tectonic and lithologic controls on bedrock channel profiles and processes in coastal California. *J. Geophys. Res.* 109, F03002. <http://dx.doi.org/10.1029/2003JF000086>.
- Dziewonski, A.M., Chou, T.A., Woodhouse, J.H., 1981. Determination of earthquake source parameters from waveform data for studies of global and regional seismicity. *J. Geophys. Res. Solid Earth* 86 (B4), 2825–2852.
- Echavarría, L., Hernandez, R., Allmendinger, R., Reynolds, J., 2003. Subandean thrust and fold belt of northwestern Argentina: Geometry and timing of the Andean evolution. *AAPG Bull.* 87 (6), 965–985.
- Ekström, G., Nettles, M., Dziewoński, A.M., 2012. The global CMT project 2004–2010: Centroid-moment tensors for 13,017 earthquakes. *Phys. Earth Planet. Inter.* 200–201, 1–9.
- Flores-Niño, J.-M., Aydin, A., Mavko, G., Anonellini, M., Ayaviri, A., 2005. Fault and fracture systems in a fold and thrust belt: An example from Bolivia. *AAPG Bull.* 89, 471–493.
- Godard, V., et al., 2012. Impact of glacial erosion on Be-10 concentrations in fluvial sediments of the Marsyandi catchment, central Nepal. *J. Geophys. Res. Earth Surf.* 117.
- Godard, V., Bourlès, D.L., Spinabella, F., Burbank, D.W., Bookhagen, B., Fisher, G.B., Moulin, A., Lézanni, L., 2014. Dominance of tectonics over climate in Himalayan denudation. *Geology* 42, 243–246. <http://dx.doi.org/10.1130/G35342.1>.
- Guarachi, H.P.S., Tawackoli, S., Salinas, W.A. and Gonzales, H.M., 2001. Mapa Geológico de Bolivia, scale 1:1,000,000. In: S.G.D.B.Y.P.F. Bolivianos (Ed.), La Paz

- Guyot, J.L., Bourges, J., Cortez, J., 1994. Sediment Transport in the Rio Grande, an Andean River of the Bolivian Amazon Drainage Basin. *IAHS* 224, 223–231.
- Guyot, J.L., Filizola, N., Quintanilla, J., Cortez, J., 1996. Dissolved solids and suspended sediment yields in the Rio Madeira basin, from the Bolivian Andes to the Amazon. *Erosion and Sediment Yield: Global and Regional Perspectives*. 236 pp. 55–63.
- Hanks, T.C., Kanamori, H., 1979. A moment magnitude scale. *J. Geophys. Res. Solid Earth* 84 (B5), 2348–2350.
- Hilley, G.E., Coutand, I., 2009. Links between topography, erosion, rheological heterogeneity, and deformation in contractional settings: Insights from the central Andes. *Tectonophysics* 495, 78–92.
- Hippe, K., et al., 2012. Quantifying denudation rates and sediment storage on the eastern Altiplano, Bolivia, using cosmogenic ¹⁰Be, ²⁶Al, and in situ ¹⁴C. *Geomorphology* 179, 58–70.
- Horton, B.K., 1999. Erosional control on the geometry and kinematics of thrust belt development in the central Andes. *Tectonics* 18, 1292–1304.
- Horton, B.K., DeCelles, P.G., 1997. The modern foreland basin system adjacent to the Central Andes. *Geology* 25 (10), 895–898.
- Hovius, N., Meunier, P., Ching-Weei, L., Hongey, C., Yue-Gau, C., Dadson, S., Ming-Jame, H., Lines, M., 2011. Prolonged seismically induced erosion and the mass balance of a large earthquake. *Earth Planet. Sci. Lett.* 304, 347–355.
- Huffman, G.J., Adler, R.F., Bolvin, D.T., Gu, G., Nelkin, E.J., Bowman, K.P., Hong, Y., Stocker, E.F., Wolff, D.B., 2007. The TRMM Multisatellite Precipitation Analysis: Quasi-Global, Multi-Year, Combined-Sensor Precipitation Estimates at Fine Scales. *J. Hydrometeorol.* 8, 38–55.
<http://www.ceresis.org>
- Insel, N., et al., 2010. Spatial and temporal variability in denudation across the Bolivian Andes from multiple geochronometers. *Geomorphology* 122 (1–2), 65–77.
- Isacks, B.L., 1988. Uplift of the Central Andean Plateau and bending of the Bolivian Orocline. *J. Geophys. Res.* 93, 3211–3231.
- Istanbulluoglu, E., Bras, R.L., 2006. On the dynamics of soil moisture, vegetation, and erosion: Implications of climate variability and change. *Water Resour. Res.* 42 (6), W06418.
- Jarvis, A., Reuter, H.I., Nelson, A., Guevara, E., 2008. Hole-filled SRTM for the globe Version 4. (available from the CGIAR-CSI SRTM 90 m Database (<http://srtm.csi.cgiar.org>)).
- Kirchner, J.W., et al., 2001. Mountain erosion over 10 yr, 10 ky, and 10 my. time scales. *Geology* 29 (7), 591–594.
- Kober, F., et al., 2009. Complex multiple cosmogenic nuclide concentration and histories in the arid Rio Lluta catchment, northern Chile. *Earth Surf. Process. Landf.* 34, 398–412.
- Kober, F., et al., 2012. Debris-flow-dependent variation of cosmogenically derived catchment-wide denudation rates. *Geology* 40 (10), 935–938.
- Korschinek, G., et al., 2010. A new value for the half-life of Be-10 by Heavy-Ion Elastic Recoil Detection and liquid scintillation counting. *Nucl. Instrum. Methods Phys. Res., Sect. B* 268 (2), 187–191.
- Korup, O., 2008. Rock type leaves topographic signature in landslide-dominated mountain ranges. *Geophys. Res. Lett.* 35, L11402. <http://dx.doi.org/10.1029/2008GL034157>.
- Korup, O., Weidinger, J.T., 2011. Rock type, precipitation, and the steepness of Himalayan threshold hillslope. In: Gloaguen, R., Ratschbacher, L. (Eds.), *Growth and Collapse of the Tibetan Plateau*. Geological Society London Special Publications London, pp. 235–249.
- Korup, O., Densmore, A.L., Schlunegger, F., 2010. The role of landslides in mountain range evolution. *Geomorphology* 120 (1–2), 77–90.
- Lamb, S., 2000. Active deformation in the Bolivian Andes, South America. *J. Geophys. Res. Solid Earth* 105 (B11), 25627–25653.
- Larsen, J.J., Montgomery, D.R., 2012. Landslide erosion coupled to tectonics and river incision. *Nature Geosci.* 5, 468–473.
- Lee, E., 2013. Korrelation zwischen Erdbeben und Denudationsraten im östlichen Rio Grande Becken der Bolivianischen Anden. Universität Potsdam, Unpubl. p. 42 (BSc Thesis).
- Leonard, M., 2010. Earthquake Fault Scaling: Self-Consistent Relating of Rupture Length, Width, Average Displacement, and Moment Release. *Bull. Seismol. Soc. Am.* 100 (5A), 1971–1988.
- Ludwig, W., Probst, J.J., 1998. River sediment discharge to the oceans: present controls and global budgets. *Am. J. Sci.* 298, 265–295.
- Lupker, M., et al., 2012. Be-10-derived Himalayan denudation rates and sediment budgets in the Ganga basin. *Earth Planet. Sci. Lett.* 333, 146–156.
- Mackey, B.H., Roering, J.J., 2011. Sediment yield, spatial characteristics, and the long-term evolution of active earthflows determined from airborne lidar and historical aerial photographs, Eel River, California. *GSA Bull.* 123, 1560–1576.
- Masek, J.G., Isacks, B.L., Gubbels, T.L., Fielding, E.J., 1994. Erosion and tectonics at the margin of continental plateaus. *J. Geophys. Res.* 99, 13941–13956.
- McQuarrie, N., 2002. The kinematic history of the central Andean fold-thrust belt, Bolivia: Implications for building a high plateau. *Geol. Soc. Am. Bull.* 114 (8), 950–963.
- Meunier, P., Hovius, N., Haines, A.J., 2008. Topographic site effects and the location of earthquake induced landslides. *Earth Planet. Sci. Lett.* 275, 221–232.
- Moglen, E., Eltahir, E.A.B., Bras, R.L., 1998. On the sensitivity of drainage density to climate Change. *Wat. Res. Research* 34 (4), 855–862.
- Molnar, P., Anderson, R.S., Anderson, S.P., 2007. Tectonics, fracturing of rock, and erosion. *J. Geophys. Res.* 112, F03014. <http://dx.doi.org/10.1029/2005JF000433>.
- Montgomery, D.R., 2001. Slope distributions, threshold hillslopes, and steady-state topography. *Am. J. Sci.* 301, 432–454.
- Montgomery, D.R., Brandon, M.T., 2002. Topographic controls on erosion rates in tectonically active mountain ranges. *Earth Planet. Sci. Lett.* 201, 481–489.
- Montgomery, D.R., Balco, G., Willett, S.D., 2001. Climate, tectonics, and the morphology of the Andes. *Geology* 29, 579–582.
- Müller, A.M., Christl, M., Lachner, J., Suter, M., Synal, H.A., 2010. Competitive Be-10 measurements below 1 MeV with the upgraded ETH-TANDY AMS facility. *Nucl. Instrum. Methods Phys. Res., Sect. B* 268 (17–18), 2801–2807.
- Ohmori, H., 1993. Changes in the Hypsometric Curve through Mountain Building Resulting from Concurrent Tectonics and Denudation. *Geomorphology* 8 (4), 263–277.
- Okada, Y., 1985. Surface deformation due to shear and tensile faults in a half-space. *Bull. Seismol. Soc. Am.* 75 (4), 1135–1154.
- Oncken, O., Boutelier, D., Dresen, G., Schemmann, K., 2012. Strain accumulation controls failure of a plate boundary zone: Linking deformation of the Central Andes and lithosphere mechanics. *Geochem. Geophys. Geosyst.* 13 (12) (n/a–n/a).
- Ouimet, W.B., Whipple, K.X., Granger, D.E., 2009. Beyond threshold hillslopes: Channel adjustment to base-level fall in tectonically active mountain ranges. *Geology* 37 (7), 579–582.
- Pepin, E., Guyot, J.L., Armijos, E., Bazan, H., Fraizy, P., Moquet, J.S., Noriega, L., Lavado, W., Pombosa, R., Vauchel, P., 2013. Climatic control on eastern Andean denudation rates (Central Cordillera from Ecuador to Bolivia). *J. South Am. Earth Sci.* 44, 85–93.
- Portenga, E.W., Bierman, P.R., 2011. Understanding Earth's eroding surface with ¹⁰Be. *GSA Today* 21 (8), 4–10.
- Rhea, S., et al., 2010. Seismicity of the earth 1900–2007, Nazca Plate and South America.
- Riebe, C.S., Kirchner, J.W., Granger, D.E., Finkel, R.C., 2001. Strong tectonic and weak climatic control of long-term chemical weathering rates. *Geology* 29 (6), 511–514.
- Roe, G.H., Montgomery, D.R., Hallet, B., 2002. Effects of orographic precipitation variations on the concavity of steady-state river profiles. *Geology* 30, 143–146.
- Roering, J.J., Perron, J.T., Kirchner, J.W., 2007. Functional relationships between denudation and hillslope form and relief. *Earth Planet. Sci. Lett.* 264, 245–258.
- Safran, E.B., et al., 2005. Erosion rates driven by channel network incision in the Bolivian Andes. *Earth Surf. Process. Landf.* 30 (8), 1007–1024.
- Scheingross, J.S., Minchew, B.M., Mackey, B.H., Simons, M., Lamb, M.P., Hensley, S., 2013. Fault-zone controls on the spatial distribution of slow-moving landslides. *GSA Bull.* 125, 473–489.
- Scherler, D., Bookhagen, B., Strecker, M.R., 2014. Tectonic control on ¹⁰Be-derived erosion rates in the Garhwal Himalaya, India. *J. Geophys. Res., Earth Surf.* 119, 83–105. <http://dx.doi.org/10.1002/2013JF002955>.
- Schmidt, K.M., Montgomery, D.R., 1995. Limits to relief. *Science* 270, 617–620.
- Schumm, S.A., Lichty, R.W., 1965. Time, space, and causality in geomorphology. *Am. J. Sci.* 263, 110–119.
- Seiler, C., Hutjes, R.W.A., Kabat, P., 2013. Climate Variability and Trends in Bolivia. *J. Appl. Meteorol. Climatol.* 52 (1), 130–146.
- Soruco, R.M., 2000. Compendio de Geología de Bolivia. *Rev. Tec. Y. P. F. B.* 18 (1–2), 1–218.
- Strahler, A.N., 1952. Hypsometric (Area-Altitude) Analysis of Erosional Topography. *Geol. Soc. Am. Bull.* 63 (11), 1117.
- Strecker, M.R., et al., 2007. Tectonics and climate of the southern central Andes. *Annu. Rev. Earth Planet. Sci.* 35, 747–787.
- Uba, C.E., Heubeck, C., Hulka, C., 2006. Evolution of the late Cenozoic Chaco foreland basin, Southern Bolivia. *Basin Res.* 18 (2), 145–170.
- Vanacker, V., von Blanckenburg, F., Govers, G., Molina, A., Poesen, J., Deckers, J., Kubik, P., 2007. Restoring dense vegetation can slow mountain erosion to near natural benchmark levels. *Geology* 35, 303–306.
- Vega, A., Buforn, E., 1991. Focal Mechanisms of Intraplate Earthquakes in Bolivia, South-America. *Pure Appl. Geophys.* 136 (4), 449–458.
- Weston, J., Ferreira, A.M.G., Funning, G.J., 2011. Global compilation of interferometric synthetic aperture radar earthquake source models: 1. Comparisons with seismic catalogs. *J. Geophys. Res. Solid Earth* 116 (B8), B08408.
- Whipple, K.X., Gasparini, N.M., 2014. Tectonic control of topography, rainfall patterns, and erosion during rapid post-12 Ma uplift of the Bolivian Andes. *Lithosphere* 27. <http://dx.doi.org/10.1130/L325.1>.
- Willenbring, J.K., Codilean, A.T., McElroy, B., 2013. Earth is (mostly) flat: Apportionment of the flux of continental sediment over millennial time scales. *Geology* 41, 343–346.
- Wittmann, H., von Blanckenburg, F., Guyot, J.L., Maurice, L., Kubik, P.W., 2009. From source to sink: Preserving the cosmogenic (¹⁰Be)-derived denudation rate signal of the Bolivian Andes in sediment of the Beni and Mamore foreland basins. *Earth Planet. Sci. Lett.* 288 (3–4), 463–474.
- Wittmann, H., von Blanckenburg, F., Maurice, L., Guyot, J.L., Filizola, N., Kubik, P.W., 2011. Sediment production and delivery in the Amazon River basin quantified by in situ-produced cosmogenic nuclides and river loads. *GSA Bull.* 123 (5–6), 934–950.
- Wobus, C., et al., 2006. Tectonics from topography: Procedures, promise, and pitfalls. *Tecto. Clim. Landsc. Evol.* 398, 55–74.
- Wolinsky, M.A., Pratson, L.F., 2005. Constraints on landscape evolution from slope histograms. *Geology* 33 (6), 477–480.
- Yanites, B.J., Tucker, G.E., Anderson, R.S., 2009. Numerical and analytical models of cosmogenic radionuclide dynamics in landslide-dominated drainage basins. *J. Geophys. Res.* 114. <http://dx.doi.org/10.1029/2008JF001088>.
- Zeilinger, G., Kober, F., Hippe, K., 2010. Correlations between morphometric parameters and catchment wide denudation rates in catchments affected by crustal bending. *Geophys. Res. Abstr.* 12, EGU2010-EGU13510.
- Zeilinger, G., Schlunegger, F., 2007. Possible flexural accommodation on the eastern edge of the Altiplano in relation to focussed erosion in the Rio La Paz drainage system. *Terra Nova* 19 (5), 373–380.